An improved cable-cylinder bracing system with quarter-ring yielding devices for seismic retrofit of steel moment frames

Oreste Bursi [a], Nader Fanaie [b*], Shervin Safaei Faegh [b]

[a] *Department of Civil, Environmental and Mechanical Engineering, University of Trento, Trento 38123, Italy*

[b] *Department of Civil Engineering, K. N. Toosi University of Technology, Tehran, Iran*

ABSTRACT

Cable-cylinder bracing system is a novel system composed of two steel cables and a steel pipe installed in a frame center. This system exhibits several merits mainly due to its simplicity; however, it needs to be enhanced due to limited source of energy dissipation, caused by plastic hinges formed at the ends of the beam, turning up some inappropriate cyclic behaviors in the hysteresis diagram of the system and also rupturing of the cables in large drifts. Therefore, we suggest the use of replaceable devices made of steel quarter-rings; and we propose a couple of accurate, practical, and simple formulas to calculate steel quarter-rings thickness utilized as replaceable devices. These equations correspond to the number of plastic hinges formed in the device partially under the capacity based design method. Also, the validity of these formulas along with the design requirements of device geometric parameters is fully examined and discussed by conducting FE-based parametric studies. Then, through the addition of four curved yielding devices made of low-yield-point steel to a cable-cylinder bracing system, the performance of the proposed system subjected to cyclic loading is identified. Based on the results, the new enhanced system represents a cost-effective,

* Corresponding author at: K. N. Toosi University of Technology, Civil Engineering Department, No. 1346, Vali-Asr Street, P.O. Box. 15875-4416, 19697 Tehran, Iran.
E-mail address: fanaie@kntu.ac.ir (N. Fanaie).

functional and competitive bracing system for retrofitting existing buildings which prevents beam-to-column connections from being subjected to direct cable forces. Finally, it can provide considerable energy dissipation, ductility along with the increase in both initial stiffness and ultimate strength and limit pinching in the case of hysteretic cycles.

Keywords: Quarter-ring device, Cable-cylinder bracing system, Method of least work, Low-yield-point steel, FE model, Plastic hinge

1. Introduction

Steel moment-resisting frames are typically recognized as flexible lateral load resisting systems that may experience large plastic deformations and drifts during a severe earthquake event. In 2007, Hou and Tagawa [1] presented a new bracing method for seismic strengthening of steel moment frames using cables and a hollow cylinder through which the cables pass at their intersections, as depicted in Fig. 1. The pipes with high or low stiffness made of steel or PVC, respectively, can be utilized for the central cylinder. The cylinder increases the lengths of cables in comparison to those of cross cable bracing. When the cylinder is rigid, it cannot be deformed; therefore, the lengths of cables do not remain constant during the lateral displacement of the frame, and the bracing members start acting from the beginning. Accordingly, the behavior of the brace should not be considered as that of ordinary cross cable bracing [1, 2].

As it is observed in Fig 1(b), when the cable-cylinder bracing frame moves as far to the right as the static lateral displacement δ, the center of the cylinder moves horizontally towards the right by $\frac{\delta}{2}$, and then the horizontal cylinder rotates

counter-clockwise by θ. The cylinder should rotate to neutralize its moment caused by the cables [3].

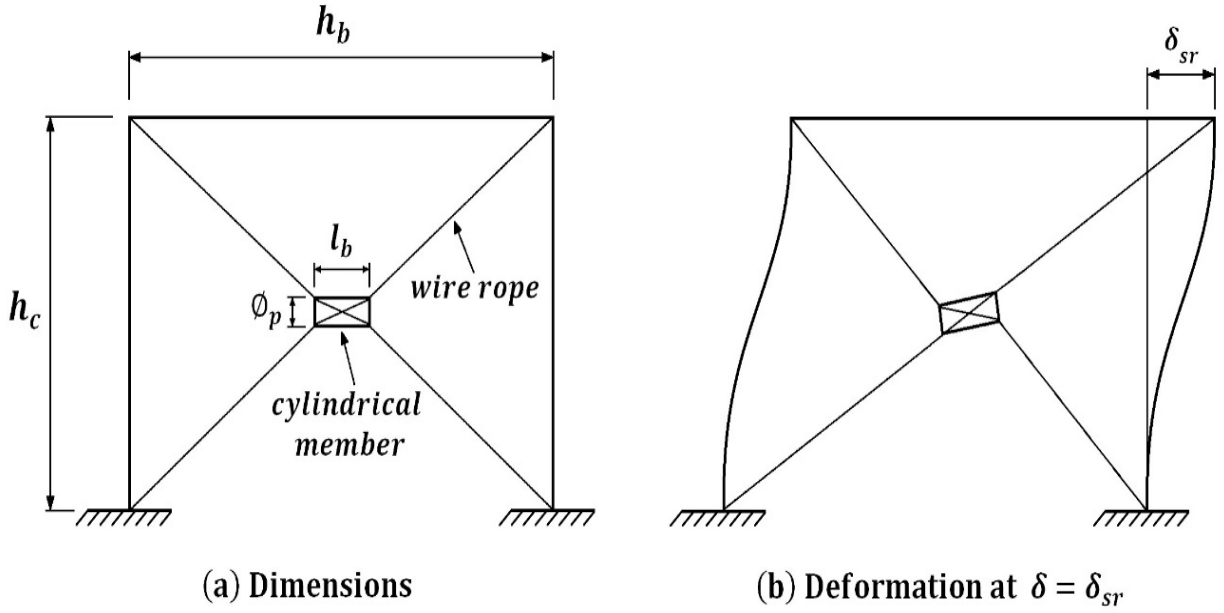

Fig. 1. Cable-cylinder bracing system: a) Geometric details; and b) deformed frame [4].

The merits of the mentioned bracing system [2, 3, 5, 6] are briefly summarized herein:

(1) Both wire ropes are under tension in a various range of loading, and none of them are loosened under lateral displacement; therefore, the impact induced by the loosening of cables is eliminated.

(2) The storeys drifts are drastically reduced regarding constant base shears, and the compressive force of the columns is less increased compared with that of the cross-cable bracing system.

(3) The stiffness of the cable-cylinder bracing system is almost zero in lower drifts. Thus, taking the period of the moment frame equipped with cable-cylinder bracing the same as the period of the moment frame would be reasonable in the lower drifts.

(4) The energy dissipation of the cable-cylinder bracing system is remarkably higher than that of the cross-cable bracing system.

(5) The smaller cross-sectional area of frame members is required for cable-cylinder bracing in comparison to that of cross-cable bracing.

(6) Cable-cylinder bracing system prevents the damages from being concentrated and accumulated in a certain storey (known as soft-storey).

In the cable-cylinder bracing with a central stiff cylinder, both bracing members are in tension due to the rotation of cylinder member. According to Fig. 2, tensile forces (T_b), appear in member b as well [2].

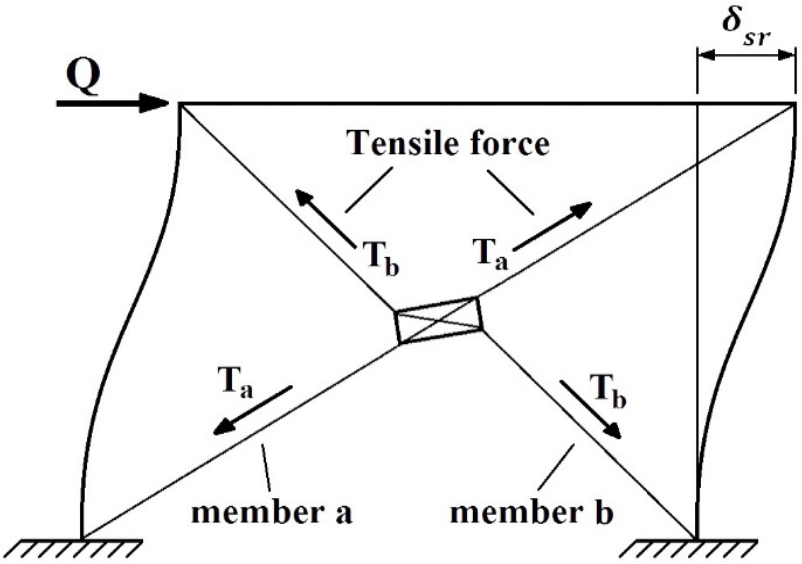

Fig. 2. Function of the cable-cylinder bracing system with a stiff cylinder [4].

Fanaie et al. [4] have also derived a set of equations governing the behavior of stiff cable-cylinder bracing (for example steel cylinders). In this research, the effects of cylinder dimensions as well as prestressing of the wire ropes on the behavior of cable-cylinder bracing have been extensively assessed. Subsequently, the force-displacement (P–δ) and strain-displacement (ε–δ) curves obtained from constitutive formulas and numerical modeling, have been compared. Fanaie and Zafari [7] by performing incremental dynamic analyses considering 10 earthquake records, came up with the overstrength factor, ductility factor, and

response modification factor of the cable-cylinder bracing system. Based on the allowable stress design method, the values of 2.33, 1.47 and 4.94 were calculated for overstrength, ductility, and response modification factors, respectively. Moreover, by conducting sensitivity analysis upon the dimensions of cylinder, including its length and internal diameter, and prestressing stress of cables, they found that under low prestressing stress condition, the response modification factor becomes larger with an increase in the length and a decrease in the diameter of the cylinder. On the other hand, the response modification factor of the system decreases with the increase in the prestressing stress of the cables.

Beheshti-Aval et al. [8] introduced the design of a new combination of friction/hysteretic device installed in the intersection of cross-bracing so as to dissipate a large amount of input seismic energy, as illustrated in Fig. 3. This interesting system includes a circular yielding ring capable of dissipating energy through steel yielding, along with slotted-bolted connections which behave as hysteretic device and work frictionally.

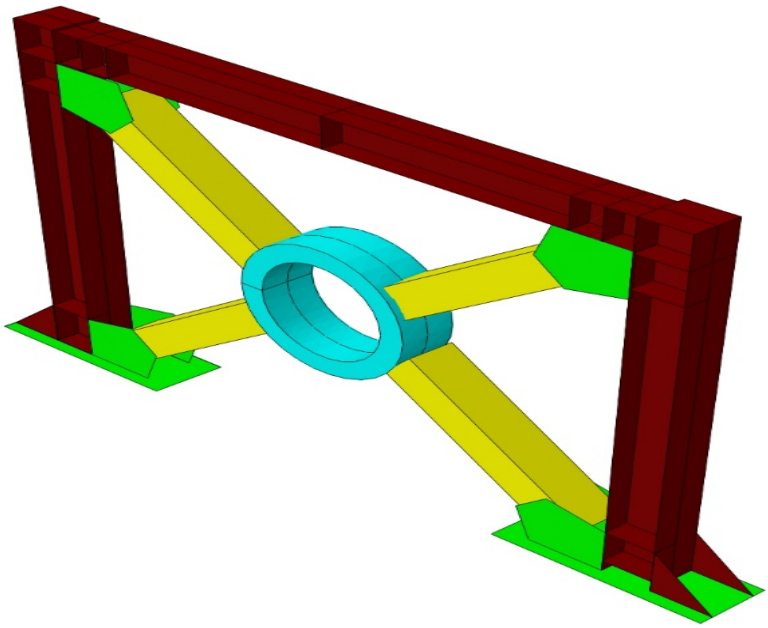

Fig. 3. A circular device inside the bracing system [8].

Deng et al. [9] developed and examined a novel crawler steel device consisting of two U-shaped steel energy dissipator plates as well as two connection plates. In this system, two U-shaped steel plates are bolted to the upper and lower connection plates with the aim of dissipating energy through the plastic deformations of the U-shaped plates. Maleki and Mahjoubi [10] suggested a new passive earthquake energy dissipative device called dual-pipe device (DPD). The proposed device has two pipes welded at designated locations, and dissipates input energy mainly through inelastic cyclic deformations. In this experimental study, all four samples of DPD exhibited excellent ductility, energy dissipation as well as stable hysteresis loops. Utomo et al. [11] carried out a finite element study on an innovative vertical steel pipe device strengthened by two trapezoidal plates attaching to the outside of the pipe and also three inner rings whose role was to stabilize the pipe cross-section. The rings were designed not to yield; however, the pipe and trapezoidal plates were designed to yield, owing to achieving an appropriate amount of energy dissipation. This pipe device experienced a large portion of cyclic yielding under cyclic loadings. Andalib et al. [12] focused on an experimental investigation upon a device ring comprised of two steel half-ring plates. The advantages of their design details for the device ring are its diversity in construction because of using bolted connection rather than welding one, and ease of installation and replacement. As reported, the device rings are capable of behaving like a fuse providing the whole system with a high level of energy dissipation, and also postponing brace buckling.

By setting up experimental and numerical studies, Taiyari et al. [13] suggested a new bracing system possessing U-shaped elements that can be employed as a hysteretic device to dissipate input energy. The experimental tests under cyclic loading corroborated the high energy dissipating capacity and stable hysteretic behavior of this bracing system. Another experimental

study conducted by Chen et al. [14] looked at using graded yield metal type of annular device in structures. The system consists of inner and outer ring metal devices with various sizes, connected along with the middle steel plates by bolts, as depicted in Fig. 4. The obtained experimental results indicated that these ring-shaped metal devices possess large deformation capacity, energy-dissipation as well as considerable anti-fatigue performance.

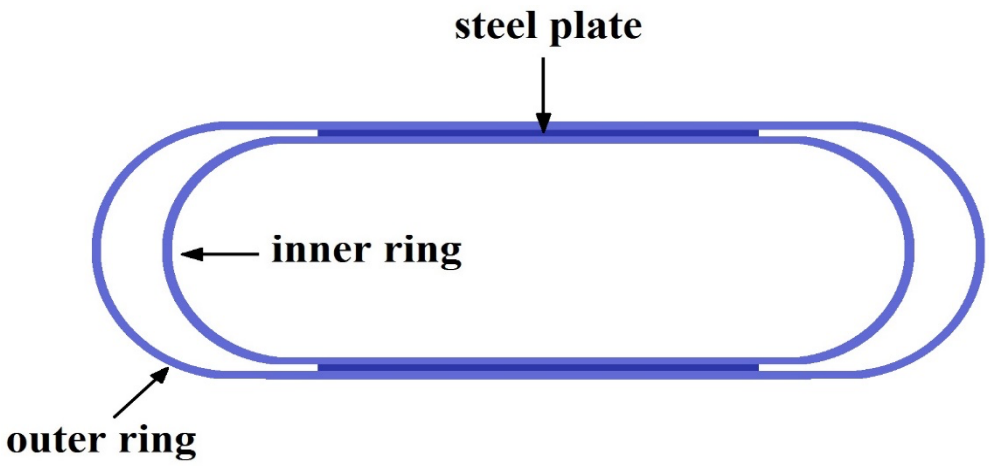

Fig. 4. Configuration of the graded yield metal device [14].

Since minimizing damages arose from an earthquake event has always been an appealing topic to scholars, employment of structural fuses equipped with low-yield-point (LYP) steel plates and installed just close to the main members is pursued by several researches ([15-18]). LYP steel plates are promising alternatives to conventional ones towards improving the structural performance of a system that is the product of exposing the conspicuous deformation capacity of such steels. On the other hand, utilizing devices made of LYP steel leads to reducing the compactness ratio of the element so that the risk of local buckling decreases accordingly.

In the current study, an innovative lateral resisting system called Ring-Cable-Cylinder bracing system has been designed and presented. Hence, by presenting a mathematical procedure employing the theorem of the least work as well as the

method of virtual work besides, a couple of exact, practical, and easy-to-use equations have been established to calculate the thickness of the quarter-ring yielding devices. In what follows, the design requirements of these curved devices according to characteristics of the frame containing them, have been addressed exhaustively. Then, the effectiveness of the recommended formulas has been comprehensively explored in the light of finite element parametric study. Ultimately, the merits that the new system is endowed by which, has been entirely specified in detail by adding designed devices to the finite element model of a tested Cable-Cylinder bracing frame.

2. Yielding devices used into the cable-cylinder bracing system

In the cable-cylinder systems, both cables along with the stiff cylinder are assumed to be elastic during loading. As a result, there is no energy dissipation in this bracing system, and the ductility of the braced moment frame is provided merely by the formation of plastic hinges at the ends of the beam. In the proposed bracing system in this research, 4 curved elements are used to connect the cables to the beam-to-column connections, as can be seen in Fig. 5. Given the usual cable-cylinder bracing system, the suggested hybrid system can alter the seismic performance of the frame and also prevent beam-to-column connections from being directly under damages in severe earthquakes, or even mitigating detrimental effects induced by wire ropes to the connections providing early-stage yielding of the devices' materials.

Since the beam and column directions are perpendicular in an ordinary frame, the angle of the curved elements should be 90 degrees for an easy installation. These curved members can be produced by dividing a steel pipe into four equal segments or forming a steel flat plate. Each curved element would be subjected to a concentrated force from the cable causing the bending moment as well as axial and shearing forces.

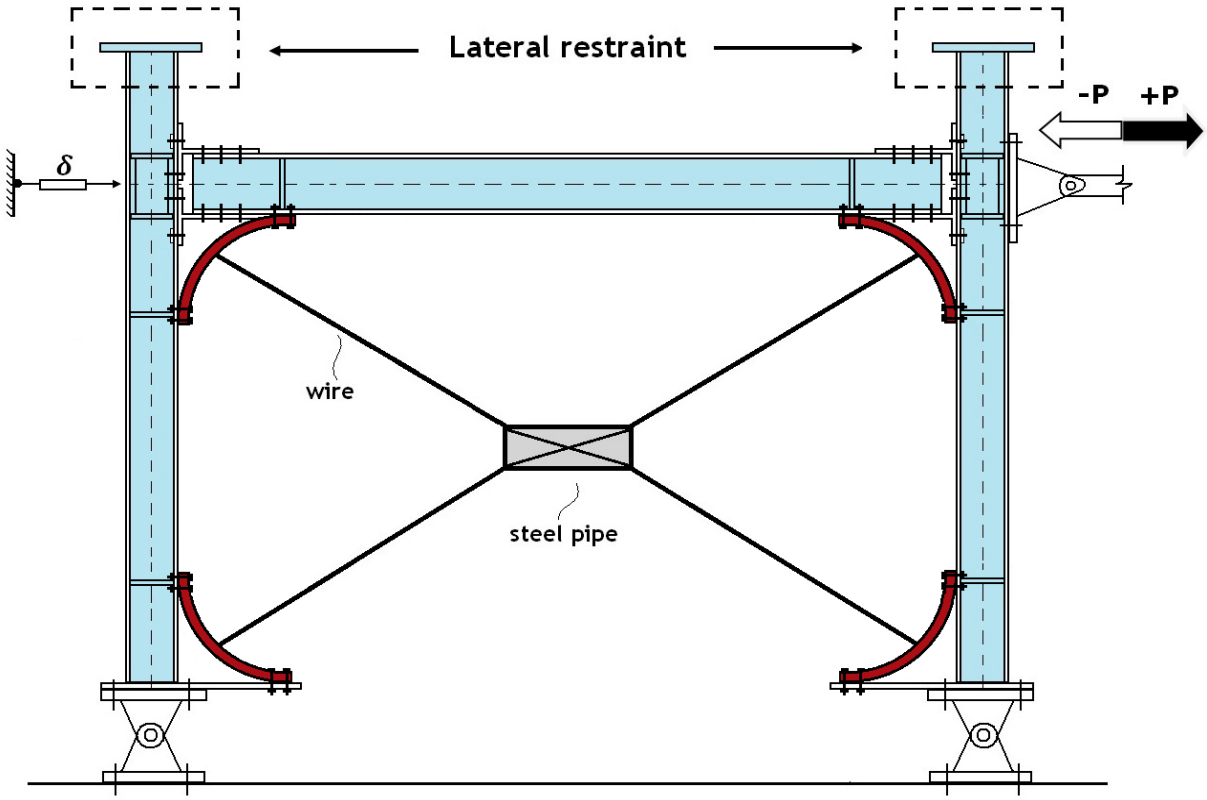

Fig. 5. Sketch of the proposed ring-cable-cylinder bracing system.

Drastic tensile forces in the cables generated by a severe earthquake result in the formation of numerous plastic hinges in the curved devices. Hence, these devices provide the system with an extra source of energy dissipation and ductility as well. Based on these facts, implementing LYP steel yielding devices in the system can help to achieve a more favorable and stable cyclic behavior. The LYP steel has a relatively lower yield point and unprecedented plastic deformation ability enabling the devices to enter the plastic phase earlier, and also remain at service under large deformations. Thus, making use of LYP steel rather than conventional structural steel in devices can enhance the energy dissipation capacity of these hysteretic devices.

Considering the tensile forces of both cables in a cable-cylinder bracing system as well as the specific curvature of the quarter-ring devices, arch action in these elements gives higher stiffness to the frame so that it enhances the stability of the

system after yielding of the curved devices in strong ground motions which is an inevitable positive point. As each curved device is connected to the frame by four bolts (two bolts for connecting to the beam flange and two for the column flange), it can be readily replaced with a new one after its yielding in a severe earthquake.

3. Analysis of the curved element with the method of least work

Owing to the special geometry and curvature of the devices, their bolted connections to beams and columns can be considered as rigid connection with a proper approximation. Therefore, each element can be analyzed as a distinct fixed-end curved member with the radius of R, as displayed in Fig. 6. Regarding this figure, under a large tensile force in wire ropes, two plastic hinges can be formed at both fixed supports of the curved element and one in the middle of the curved element in which the concentrated tensile force of *F* is applied. These three plastic hinges dissipate energy during a severe earthquake event and increase the ductility level of the system.

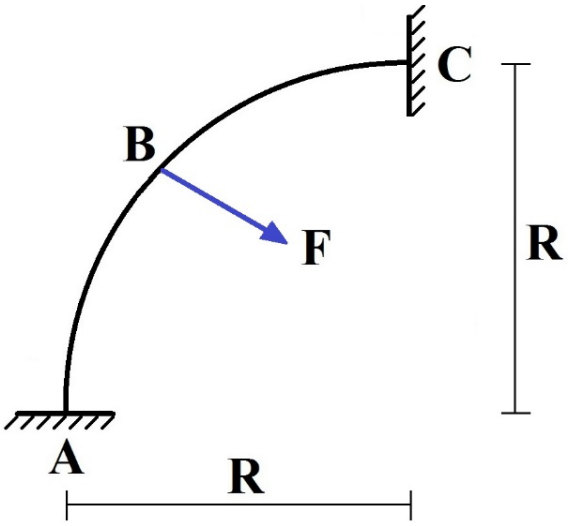

Fig. 6. Fixed both ends curved device subjected to a general tensile force.

The angle of applied tensile force to the curved element depends on the beam length, column height, internal diameter and length of the central cylinder. In each desired frame, it is easy and possible to adjust the cables angles to 45° (in the radial direction of the curved element) by doing trial and error on the length and internal diameter of the central cylinder, as depicted in Fig. 7. However, if the cable is not located in a radial direction, its tensile force can be resolved into two components of radial and tangential directions. The tangential component is considered as an anti-symmetric loading for the curved device. Consequently, it does not cause any bending moment in the middle of the curved element because of the property of symmetric structures subjected to anti-symmetric loading. Also, it should be noted that axial forces throughout the curved element do not play a significant role in the elastic analysis of this element, unlike plastic analysis. Therefore, the bending moment at the middle of the curved device is produced merely by the radial component of the tensile force. Due to symmetry in the geometry as well as loading of the above-mentioned curved element, it can be replaced with an equivalent curved half-element, represented in Fig. 8, and then analyzed.

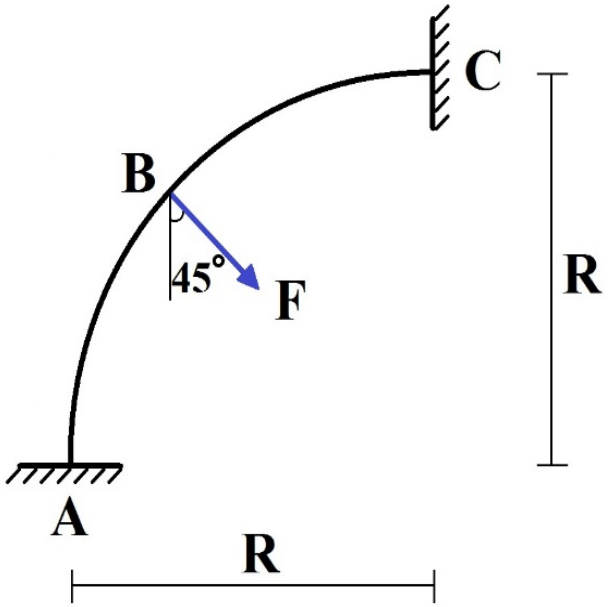

Fig. 7. Fixed both ends curved device subjected to a central tensile force in 45° direction.

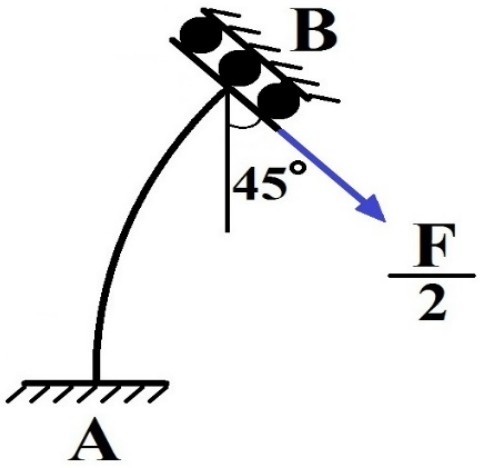

Fig. 8. Equivalent curved half-element.

The curved structure illustrated in Fig. 8, is hyperstatic. Thus, it cannot be analyzed using routine static equations. Given the support conditions, the half-element has two redundancies making it two degrees indeterminate system. The bending moment and shearing force in the fixed support are denoted as M_O and V_O. Fig.9 shows that the axial force in the fixed support, S_O, is calculated (by Eq. (1)) using an equilibrium equation in the direction of the applied oblique force of $F/2$.

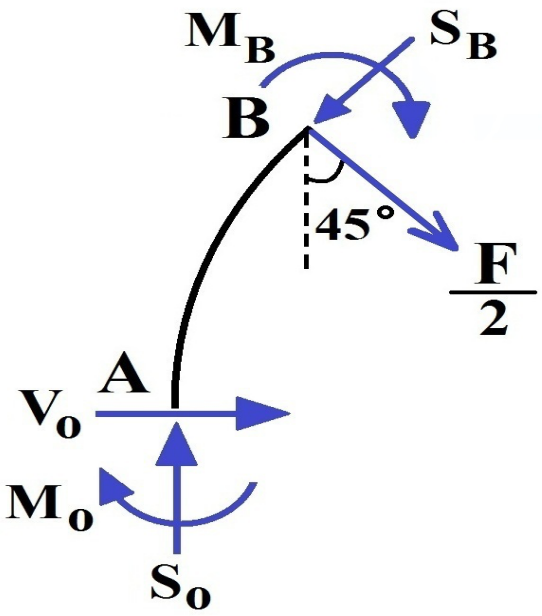

Fig. 9. Free body diagram of the curved half-element.

$$\sum F = 0 \rightarrow S_0 \cos 45 - V_0 \cos 45 = \frac{F}{2} \rightarrow \frac{\sqrt{2}}{2}(S_0 - V_0) = \frac{F}{2} \rightarrow$$
$$S_0 - V_0 = \frac{\sqrt{2}}{2} F \rightarrow S_0 = \frac{\sqrt{2}}{2} F + V_0 \quad (1)$$

As depicted in Fig. 10, bending moment in the optional angle of θ can be calculated by writing a moment equilibrium equation about optional node D.

$$\sum M = 0 \rightarrow M(\theta) - V_0 R \sin\theta + S_0 R(1-\cos\theta) + M_0 = 0$$
$$\rightarrow M(\theta) = -M_0 + V_0 R \sin\theta - S_0 R(1-\cos\theta)$$
$$= -M_0 + V_0 R \sin\theta - (\frac{\sqrt{2}}{2} F + V_0) R(1-\cos\theta) \quad (2)$$
$$= -M_0 + V_0 R \sin\theta - \frac{\sqrt{2}}{2} FR(1-\cos\theta) - V_0 R(1-\cos\theta)$$
$$\rightarrow M(\theta) = -M_0 - V_0 R(1-\sin\theta-\cos\theta) - \frac{\sqrt{2}}{2} FR(1-\cos\theta)$$

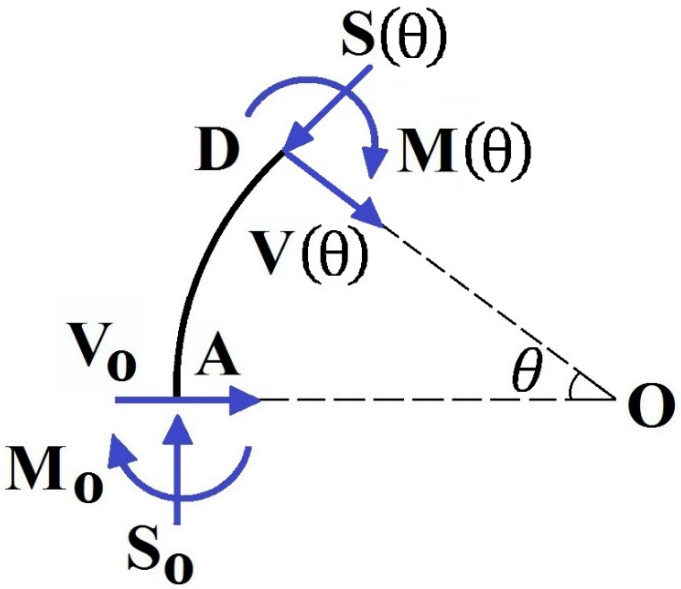

Fig. 10. Free body diagram of the curved half-element corresponding to angle of θ.

The two useful derivatives expressed in Eqs. (3) and (4) will be needed in the following.

$$\frac{\partial M(\theta)}{\partial M_0} = -1 \quad (3)$$

$$\frac{\partial M(\theta)}{\partial V_0} = -R(1-\sin\theta-\cos\theta) \tag{4}$$

The total strain energy due to the flexural deformations in the half-element is presented as follows:

$$U = \int_0^{\frac{\pi}{4}} \frac{M^2(\theta)}{2EI} R d\theta \tag{5}$$

Where E is the modulus of elasticity of the device's material, and I is the moment of inertia of the device about the bending axis (weak axis). The virtual work method along with the method of least work, are two of the well-known, powerful, and rigorous approaches in structural analysis by which several structural analysis problems in the indeterminate systems have been addressed in previous studies [19, 20]. Based on the method of least work, the total strain energy should be minimized in terms of two independent parameters of M_O and V_O. Using this method leads to the following equations:

$$\begin{aligned}
&\frac{\partial U}{\partial M_0} = 0 \rightarrow \frac{\partial}{\partial M_0}\left[\int_0^{\frac{\pi}{4}} \frac{M^2(\theta)}{2EI} R d\theta\right] \rightarrow \int_0^{\frac{\pi}{4}} M(\theta)\frac{\partial M(\theta)}{\partial M_0} d\theta = 0 \\
&\rightarrow \int_0^{\frac{\pi}{4}} \left[-M_0 - V_0 R(1-\sin\theta-\cos\theta) - \frac{\sqrt{2}}{2} FR(1-\cos\theta)\right] \times (-1) \times d\theta = 0 \\
&\rightarrow \left[-M_0\theta - V_0 R(\theta+\cos\theta-\sin\theta) - \frac{\sqrt{2}}{2} FR(\theta-\sin\theta)\right]_0^{\frac{\pi}{4}} = 0 \\
&\rightarrow -M_0\frac{\pi}{4} - V_0 R(\frac{\pi}{4}) - \frac{\sqrt{2}}{2} FR(\frac{\pi}{4}-\frac{\sqrt{2}}{2}) + V_0 R = 0 \\
&\rightarrow \frac{\pi}{4} M_0 + V_0 R(\frac{\pi}{4}-1) = -\frac{\sqrt{2}}{2} FR(\frac{\pi}{4}-\frac{\sqrt{2}}{2})
\end{aligned} \tag{6}$$

$$\begin{aligned}
&\frac{\partial U}{\partial V_0} = 0 \rightarrow \frac{\partial}{\partial V_0}\left[\int_0^{\frac{\pi}{4}} \frac{M^2(\theta)}{2EI} R d\theta\right] \rightarrow \int_0^{\frac{\pi}{4}} M(\theta)\frac{\partial M(\theta)}{\partial V_0} d\theta = 0 \\
&\rightarrow \int_0^{\frac{\pi}{4}} \left[-M_0 - V_0 R(1-\sin\theta-\cos\theta) - \frac{\sqrt{2}}{2} FR(1-\cos\theta)\right] \times \left[-R(1-\sin\theta-\cos\theta)\right] d\theta = 0 \\
&\rightarrow \int_0^{\frac{\pi}{4}} \left[M_0(1-\sin\theta-\cos\theta) + V_0 R(1-\sin\theta-\cos\theta)^2 + \frac{\sqrt{2}}{2} FR(1-\cos\theta)(1-\sin\theta-\cos\theta)\right] d\theta = 0
\end{aligned} \tag{7}$$

To calculate the integral of Eq. (7), the following integrals need to be determined one by one:

$$\int_0^{\frac{\pi}{4}}(1-\sin\theta-\cos\theta)d\theta=\left[\theta+\cos\theta-\sin\theta\right]_0^{\frac{\pi}{4}}=\frac{\pi}{4}-1 \tag{8}$$

$$\begin{aligned}&\int_0^{\frac{\pi}{4}}(1-\sin\theta-\cos\theta)^2 d\theta=\int_0^{\frac{\pi}{4}}(1+\sin^2\theta+\cos^2\theta-2\sin\theta-2\cos\theta+2\sin\theta\cos\theta)d\theta=\\&\int_0^{\frac{\pi}{4}}(2-2\sin\theta-2\cos\theta+\sin 2\theta)d\theta=\left[2\theta+2\cos\theta-2\sin\theta-0.5\cos 2\theta\right]_0^{\frac{\pi}{4}}=\frac{\pi-3}{2}\end{aligned} \tag{9}$$

$$\begin{aligned}&\int_0^{\frac{\pi}{4}}(1-\cos\theta)(1-\sin\theta-\cos\theta)d\theta=\int_0^{\frac{\pi}{4}}(1-\sin\theta-\cos\theta-\cos\theta+\sin\theta\cos\theta+\cos^2\theta)d\theta=\\&\int_0^{\frac{\pi}{4}}(1-\sin\theta-2\cos\theta+\frac{1}{2}\sin 2\theta+\frac{1+\cos 2\theta}{2})d\theta=\int_0^{\frac{\pi}{4}}(\frac{3}{2}-\sin\theta-2\cos\theta+\frac{1}{2}\sin 2\theta+\frac{1}{2}\cos 2\theta)d\theta\\&=\left[1.5\theta+\cos\theta-2\sin\theta-0.25\cos 2\theta+0.25\sin 2\theta\right]_0^{\frac{\pi}{4}}\\&=(\frac{3\pi}{8}+\frac{\sqrt{2}}{2}-\sqrt{2}+\frac{1}{4})-(1-\frac{1}{4})=\frac{3\pi}{8}-\frac{\sqrt{2}}{2}+\frac{1}{4}-\frac{3}{4}=\frac{3\pi}{8}-\frac{\sqrt{2}}{2}-\frac{1}{2}\end{aligned} \tag{10}$$

By incorporating the integrals calculated in Eqs. (8), (9) and (10) into Eq. (7), the following equation is developed:

$$\begin{aligned}&(\frac{\pi}{4}-1)M_0+V_0R(\frac{\pi-3}{2})+\frac{\sqrt{2}}{2}FR(\frac{3\pi}{8}-\frac{\sqrt{2}}{2}-\frac{1}{2})=0\\&\rightarrow(\frac{\pi}{4}-1)M_0+V_0R(\frac{\pi-3}{2})=-\frac{\sqrt{2}}{2}FR(\frac{3\pi}{8}-\frac{\sqrt{2}}{2}-\frac{1}{2})\end{aligned} \tag{11}$$

As observed, Eqs. (6) and (11) include two variables, namely M_O and V_O in terms of external loading of F and the radial of R, which can be calculated by solving these equations. Consequently, the bending moment, shearing, and axial forces of the fixed support shown in Fig. 9 are expressed as follows:

$$M_0=0.0505FR \quad , \quad V_0=0.443F \quad , \quad S_0=1.15F \tag{12}$$

Considering the variable bending moment equation of Eq. (2), the bending moment and compressive axial force at sliding support of B (corresponding to $\theta = 45°$ depicted in Fig.9), are defined by Eq. (13) and (14), respectively:

$$M(\theta) = -M_0 - V_0 R(1 - \sin\theta - \cos\theta) - \frac{\sqrt{2}}{2} FR(1 - \cos\theta) \quad , \quad M_0 = 0.0505FR \quad , \quad V_0 = 0.443F$$

$$\rightarrow M_B = M(\theta = 45°) = -0.0505FR - 0.443FR(1 - \frac{\sqrt{2}}{2} - \frac{\sqrt{2}}{2}) - \frac{\sqrt{2}}{2} FR(1 - \frac{\sqrt{2}}{2}) = -0.0741FR \quad (13)$$

$$S(\theta = \cos 45°) = S_B, \quad \sum F = 0 \rightarrow S_B - V_0 \cos 45° - S_0 \cos 45° = 0 \rightarrow S_B = (S_0 + V_0)\cos 45° = (1.15F + 0.443F)\cos 45° = 1.126F \quad (14)$$

It can be concluded that the bending moment in joint B is slightly more than that of fixed support A. As a result, the first plastic hinge is probably formed at the point of the central tensile force.

4. Design parameters and evaluation of the curved device thickness based on one plastic hinge formation

In the new system of cable-cylinder bracing with the curved yielding devices, these curved elements should be designed based on the two separate approaches, namely the first hinge formation and the ultimate strength modes. The first approach that is completely discussed in this section evaluates the thickness of the yielding device when the connected cable's force causes the formation of the first plastic hinge merely.

In line with the objective of using the yielding devices, it is assumed that these elements are made of LYP steel with the uniaxial yield stress of F_y. Moreover, the width of the curved element, b, can be taken as that of beam flange (b_f), and should not exceed 1.25 b_f. There are two other parameters in the curved element. The first one is the radius of the curved element (R), which can be considered from 200 mm to 500 mm, and the second one is the thickness of the curved

element, t. Noted that the thickness of the curved element should be limited to minimum flange thickness of the beam and column to which the ring is attached. But the exact value of this parameter will be determined subsequently.

To design the thickness of the device, the tensile force of cable applied to the middle of the curved element, needs to be calculated. The tensile force of cable, F_1, should be calculated by exposing the braced frame to the lateral force induced by an earthquake event. Under this tensile force, the curved device experiences a compressive force as well as a considerable bending moment in node B. While the axial compressive force is approximately equal in nodes A and B, the bending moment is greater in node B. Therefore, sliding support of B is a critical point which requires to be controlled in assessing the thickness. To determine the thickness of the curved device, the following axial load-bending moment interaction equation presented by Chen and Han [21], should be implemented in this node:

$$\frac{M}{M_0} + (\frac{N}{N_0})^2 = 1 \tag{15}$$

Where $M_0=M_P$ and N_0 are the limit moment in pure bending (plastic bending moment), and the limit force in simple tension or compression (yield strength), respectively. M_0 and N_0 are defined as follows:

$$M_0 = M_p = ZF_y = \frac{bt^2}{4}F_y, N_0 = AF_y = btF_y \tag{16}$$

In which, Z is the device's plastic section modulus (for rectangular sections is equal to $\frac{bt^2}{4}$), and A is the sectional area of the quarter-ring device. Ultimately, the thickness of curved device corresponding to the first plastic hinge force (F_1), is calculated utilizing the above-mentioned interaction equation in the critical point of B:

$$\frac{M}{M_0}+(\frac{N}{N_0})^2=1 \quad , \quad M_B=-0.0741F_1R \quad , \quad S_B=1.126F_1$$
$$\rightarrow \frac{0.0741F_1R}{\frac{bt^2}{4}F_y}+(\frac{1.126F_1}{btF_y})^2=1 \rightarrow \frac{F_1}{bt^2F_y}[4\times 0.0741R+\frac{(1.126)^2F_1}{bF_y}]=1$$
$$\rightarrow \frac{F_1}{bt^2F_y}[0.296R+\frac{1.268F_1}{bF_y}]=1 \qquad (17)$$
$$\rightarrow t=\sqrt{\frac{F_1}{bF_y}[0.296R+\frac{1.268F_1}{bF_y}]}$$

5. Evaluation of the device thickness based on the capacity-based design method

This section aims to derive practical and precise formulas to calculate maximum strength of the quarter-ring devices resulting from developing three plastic hinges along with axial forces internal work using mathematical procedures as well as virtual work method. Then, by equalizing the maximum strength of the device with the tensile yield strength of the cables (according to the capacity based design method), the unknown thickness of the devices is obtained in the desired design.

In the quarter-ring arc illustrated in Fig. 11, assuming that three bending plastic hinges would be formed at three nodes, A, B, and C, and also the middle node B would experience an inward radial displacement equals to Δ; accordingly, the horizontal and vertical displacement components of node B will be equal to $\frac{\sqrt{2}}{2}\Delta$. The two arcs AB and CB belonged to a circle with the center O and the radius of *R*, have presumably radii the same as *R* subsequent to the formation of the plastic hinges. However, their arc angles are no longer equal to $\frac{\pi}{4}$ and will be less. The assumption that states the two new arcs remain circles with the radius of *R* is almost correct due to ignoring the bending and shearing deformations of the

primary arc caused by displacement Δ, but this assumption needs to be modified at the end of this section. In this case, the center of curvature for arcs AB′ and CB′ is no longer the point O and will become O′ and O″, respectively (Fig. 1).

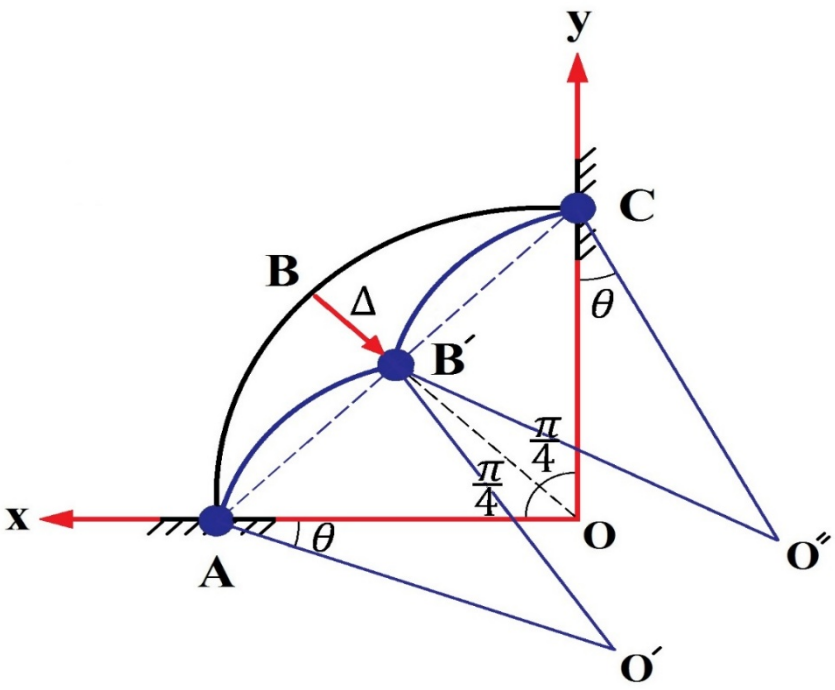

Fig. 11. Deformation of the quarter-ring device under an applied radial force with 45 degrees.

Consequently, each of the arcs AB and CB has experienced a decrease in their length due to compressive axial forces and turned into the arcs AB′ and CB′. To accurately tackle this problem with no change in the x-y coordinate system (the radius OA is the x-axis and the radius OB is the y-axis), the coordinates of new arcs centers (i.e. points O′ and O″), need to be calculated so as to be utilized in the virtual work method. Owing to the existing approximately equal axial forces throughout the length of the primary arc as well as the same reduction in the length of the arc AB as the arc CB due to the symmetry of the problem, the calculation can be merely focused on the arc AB and then obtained results can be

extended to the arc CB as well. The equation of the initial circle in the x-y coordinate system (before deformation), is presented as follows:

$$x^2 + y^2 = R^2 \tag{18}$$

If node B directly moves towards the center of O in the value of Δ, given that the radial extension of BB′ makes the angle of 45 degrees with the x and y axes, the coordinates of new point B′are determined as:

$$x_{B'} = y_{B'} = (R - \Delta)\sin 45 = \frac{\sqrt{2}}{2}(R - \Delta) \tag{19}$$

If the center of curvature of the arc AB′ is considered the point O′ and it is assumed that the coordinates of this new curvature center are $O' \left|{}^{\alpha}_{\beta}\right.$, that is the center of a circle with the radius of *R*, the equation of arc AB′ would be expressed as Eq. (20). In addition, the coordinates of both points A and B′ need to satisfy this equation.

$$AB' : (x-\alpha)^2 + (y-\beta)^2 = R^2 \tag{20}$$

$$A : \begin{bmatrix} x_A = R \\ y_A = 0 \end{bmatrix} \rightarrow (R-\alpha)^2 + (0-\beta)^2 = R^2 \rightarrow R^2 - 2R\alpha + \alpha^2 + \beta^2 = R^2$$

$$\rightarrow \alpha^2 - 2R\alpha + \beta^2 = 0 \tag{21}$$

$$\rightarrow \alpha^2 + \beta^2 = 2R\alpha \tag{22}$$

$$B' : \begin{bmatrix} x_{B'} = \frac{\sqrt{2}}{2}(R-\Delta) \\ y_{B'} = \frac{\sqrt{2}}{2}(R-\Delta) \end{bmatrix} \rightarrow [\frac{\sqrt{2}}{2}(R-\Delta) - \alpha]^2 + [\frac{\sqrt{2}}{2}(R-\Delta) - \beta]^2 = R^2$$

$$\rightarrow \frac{1}{2}(R-\Delta)^2 - \sqrt{2}(R-\Delta)\alpha + \alpha^2 + \frac{1}{2}(R-\Delta)^2 - \sqrt{2}(R-\Delta)\beta + \beta^2 = R^2 \rightarrow$$

$$(R-\Delta)^2 - \sqrt{2}(R-\Delta)(\alpha+\beta) - R^2 + \alpha^2 + \beta^2 = 0 \rightarrow$$

$$R^2 - 2R\Delta + \Delta^2 - \sqrt{2}(R-\Delta)(\alpha+\beta) - R^2 + \alpha^2 + \beta^2 = 0 \rightarrow$$

$$\Delta^2 - 2R\Delta - \sqrt{2}(R-\Delta)(\alpha+\beta) + \alpha^2 + \beta^2 = 0 \tag{23}$$

By replacing of $\alpha^2 + \beta^2$ with $2R\alpha$ (obtained from Eq. (22)) in Eq. (23), this equation is redefined as follows:

$$\Delta^2 - 2R\Delta - \sqrt{2}(R-\Delta)(\alpha+\beta) + 2R\alpha = 0 \tag{24}$$

The values of α and β are determined from Eqs. (21) and (24) in terms of radius R and displacement Δ, and then the coordinates of the center of the new circle, O', is ultimately calculated. For this purpose, the value of β in terms of R and α in Eq. (21) is calculated and incorporated in Eq. (24):

$$\alpha^2 - 2R\alpha + \beta^2 = 0 \rightarrow \beta^2 = 2R\alpha - \alpha^2 \rightarrow \beta = -\sqrt{2R\alpha - \alpha^2} \tag{25}$$

$$\begin{aligned} &\beta = -\sqrt{2R\alpha - \alpha^2} \rightarrow \Delta^2 - 2R\Delta - \sqrt{2}(R-\Delta)(\alpha - \sqrt{2R\alpha - \alpha^2}) + 2R\alpha = 0 \\ &\rightarrow \Delta^2 - 2R\Delta - \sqrt{2}\alpha(R-\Delta) + \sqrt{4R\alpha - 2\alpha^2}\,(R-\Delta) + 2R\alpha = 0 \\ &\rightarrow \Delta^2 - 2R\Delta - \sqrt{2}\alpha(R-\Delta) + 2R\alpha = -\sqrt{4R\alpha - 2\alpha^2}\,(R-\Delta) \end{aligned} \tag{26}$$

It needs to be mentioned that the vertical coordinate of the $O'$is negative since it is under the x-axis. Using Eq. (26) the longitudinal coordinate of α is achieved in terms of the parameters R and Δ. On the other hand, in case of difficulty in solving Eq. (26) despite having R and Δ values, it is possible to estimate the approximate value of α through solving the following second-order equation in which the right-hand side is only a numerical value:

$$\sqrt{4R\alpha - 2\alpha^2} = \frac{2R\Delta}{R-\Delta} \tag{27}$$

After determining the values of α and β, as depicted in Fig. 12, the central angle of the new arc, $AO'B'$, should be calculated using trigonometry rules

presented in Eq. (28) so that using the value of this reduced angle (relative to 45 degrees), γ, leads to evaluate the reduction in length in AB and CB arcs.

$$\frac{AB'}{\sin\gamma}=\frac{R}{\sin(\frac{\pi}{2}-\frac{\gamma}{2})}=\frac{R}{\cos\frac{\gamma}{2}}\rightarrow\frac{\sin\gamma}{\cos\frac{\gamma}{2}}=\frac{AB'}{R}\rightarrow\frac{2\sin\frac{\gamma}{2}\cos\frac{\gamma}{2}}{\cos\frac{\gamma}{2}}=2\sin\frac{\gamma}{2}=\frac{AB'}{R} \quad (28)$$

$$\rightarrow\sin\frac{\gamma}{2}=\frac{AB'}{2R}$$

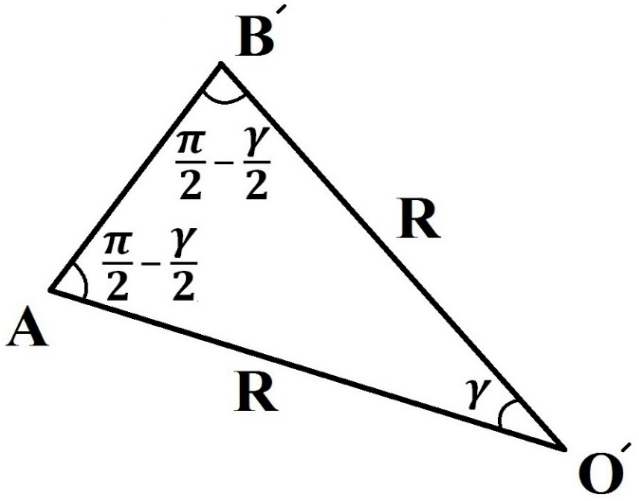

Fig. 12. Determining the angle AO′B′ using trigonometry rules.

The length of arc AB′ is calculated as follows:

$$A\begin{bmatrix}x_A=R\\y_A=0\end{bmatrix},\ B'\begin{bmatrix}x_{B'}=\frac{\sqrt{2}}{2}(R-\Delta)\\y_{B'}=\frac{\sqrt{2}}{2}(R-\Delta)\end{bmatrix}\rightarrow\left|\mathrm{AB}'\right|=\sqrt{[\frac{\sqrt{2}}{2}(R-\Delta)-R]^2+[\frac{\sqrt{2}}{2}(R-\Delta)]^2}=$$

$$\sqrt{\frac{1}{2}(R-\Delta)^2-\sqrt{2}R(R-\Delta)+R^2+\frac{1}{2}(R-\Delta)^2}=\sqrt{(R-\Delta)^2-\sqrt{2}R(R-\Delta)+R^2} \quad (29)$$

$$=\sqrt{R^2-2R\Delta+\Delta^2-\sqrt{2}R^2+\sqrt{2}R\Delta+R^2}=\sqrt{(2-\sqrt{2})R^2-(2-\sqrt{2})R\Delta+\Delta^2}$$

$$\simeq\sqrt{2-\sqrt{2}}\times\sqrt{R^2-R\Delta}\simeq\sqrt{2-\sqrt{2}}\,(R-\frac{\Delta}{2})$$

Consequently, Eq. (28) is rewritten as Eq. (30):

$$\sin\frac{\gamma}{2}=\frac{AB'}{2R}=\frac{\sqrt{2-\sqrt{2}}(R-\frac{\Delta}{2})}{2R}=\sqrt{2-\sqrt{2}}(\frac{1}{2}-\frac{\Delta}{4R})\rightarrow$$

$$\frac{\gamma}{2}=\arcsin[\sqrt{2-\sqrt{2}}(\frac{1}{2}-\frac{\Delta}{4R})]\rightarrow\gamma=2\arcsin[\sqrt{2-\sqrt{2}}(\frac{1}{2}-\frac{\Delta}{4R})] \quad (30)$$

Ultimately, the length reduction values in each of the arcs AB and CB are calculated using Eq. (31).

$$\Delta L_{AB}=\Delta L_{BC}=\Delta\gamma\times R=(\frac{\pi}{4}-\gamma)R=(\frac{\pi}{4}-2\arcsin[\sqrt{2-\sqrt{2}}(\frac{1}{2}-\frac{\Delta}{4R})])R \quad (31)$$

It is noteworthy that the response drawn from the arcsine term in Eq. (31) must be converted into radian, then subtracted from $\frac{\pi}{4}$. The virtual work relationship requires the reduction in length of the arcs AB and CB resulting from Eq. (31) so as to calculate the maximum radial load corresponding to the primary arc mechanism (i.e. induced by the formation of three plastic hinges at fixed ends and middle of the arc, along with axial forces internal work). Considering the axial force amount in the middle of the primary arc determined to be equal to $S_B = 1.126F$ in the previous section, as well as the rotation of plastic hinges at A and C supports to be equal to θ and the rotation of the plastic hinge at node B equals to 2θ as illustrated in Fig. (13), the relationship between internal and external work done in the quarter-ring device is written as follows:

$$4M_P\times\theta+2S_B\times\Delta L=F_2\times\Delta\rightarrow 4M_P\times\theta+2\times1.126F_2(\frac{\pi}{4}-\gamma)R=F_2\times\Delta \quad (32)$$

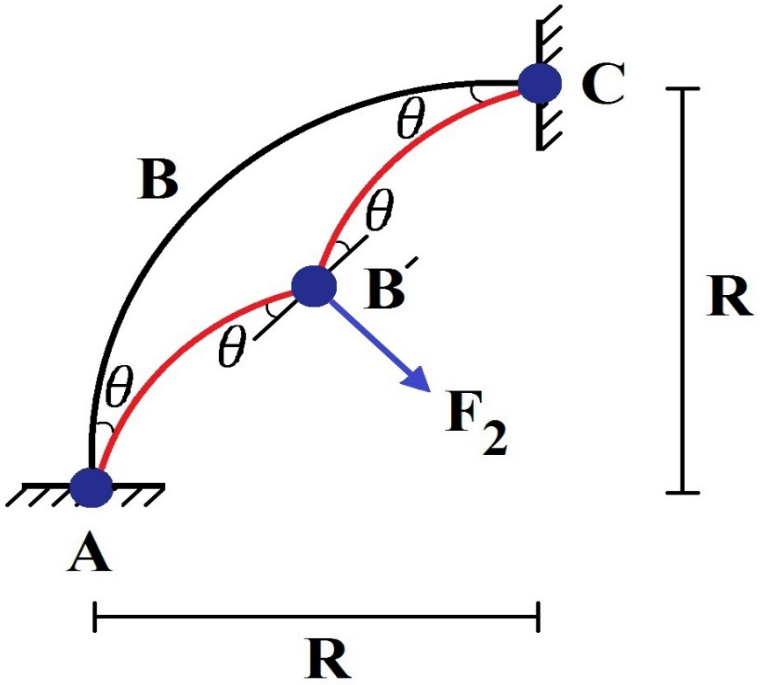

Fig. 13. Foreseen mechanism in the desired device after the formation of 3 plastic hinges.

Note that although the axial force varies along the arcs AB and CB, the variations are trivial. Therefore, by ignoring a small amount of error, the axial force of point B is used to write the virtual work relationship in Eq. (32). In this equation, F_2 is the device's ultimate strength or radial force applied to its center, in other words, it is the radial component of the force caused by tensile yielding of the cable connected to the device according to the capacity based design method. This issue reveals that the device and its cable simultaneously reach their ultimate capacity.

One of the most important points which needs to be paid special attention to is that although the force F_2 is considered to be equal to the radially connected wire rope force, the wire rope force may not be in the central direction of the device in all circumstances, like finite element model presented in Fig. 18(a). In this inevitable case occurred in frames, the virtual work relationship developed in Eq.

(32) is still applicable provided that the force F_2 is radial component of the applied cable force. When the cable force acts along the desired direction to the middle of the quarter-ring device, it can be resolved into the radial and tangential force components, but note that the tangential component has no effect on the virtual work relationship in Eq. (32). The reason is that the tangential component of the cable force is considered as anti-symmetrical loading for the device, and the amount of internal work done by it is equal to zero. Note that there is no bending moment in the middle of the device under the anti-symmetrical tangential force applied to this point. Clamping moments in the fixed supports are produced in the same direction, but due to opposite rotations of the supports (clockwise rotation of support A versus counterclockwise rotation of support C), the virtual work related to these clamping moments neutralize each other as well. On the other hand, the anti-symmetrical tangential component of the cable force creates tensile force in one half of the arc and alike compressive force in another half. This will neutralize the effects of the aforementioned tensile and compressive axial forces on the second term in the left part of Eq. (32) (related to work done by axial force); therefore, the tangential component of the cable force does not affect Eq. (32) at all. As stated before, if the cable force is not radially applied to the quarter-ring device, the only adjustment is to determine the radial component of the cable force and utilize it instead.

In what follows, the solution to the problem will be presented in two exact and approximate (with very few errors) methods.

5.1. Exact solution

In the exact solution, the rotation angle of plastic hinges in the fixed supports A and C (illustrated in Fig.11), i.e. θ, is taken to be equal to $\sin\theta$ since θ has a slight amount and this angle (in radian) can be replaced by $\sin\theta$:

$$\theta = \sin\theta = \frac{|y_{O'}|}{O'A} \ , y_{O'} = \beta = -\sqrt{2R\alpha - \alpha^2} \ , O'A = R \rightarrow \theta = \sin\theta = \frac{\sqrt{2R\alpha - \alpha^2}}{R} \quad (33)$$

Thus, Eq. (32) is redefined as follows:

$$4M_P \times \frac{\sqrt{2R\alpha - \alpha^2}}{R} + 2.252F_2R(\frac{\pi}{4} - 2\arcsin[\sqrt{2-\sqrt{2}}(\frac{1}{2} - \frac{\Delta}{4R})] = F_2\Delta \quad (34)$$

As previously mentioned, the flexural and shearing deformations of the primary arc have been ignored against the displacement Δ .In addition, the secondary arcs AB′ and CB′ have been considered as circular arcs with the radius of R, whereas, according to Fig. 14, these arcs have undergone plastic deformations and they are not exactly complete circles. The steel quarter-ring depicted in Fig. 14, with geometric characteristics of R=500 mm, b=150 mm, and t=10 mm is modeled using ABAQUS finite elements software [22]. In modeling, second-order iso-parametric eight-noded quadrilateral thick shell element with reduced integration (S8R) is employed, which is capable of considering shearing deformations in thick shell plates. Reduced integration usually provides more accurate results and dramatically reduces analysis time, especially in three-dimensional models. The yield stress of 240 MPa, the elastic modulus of E = 200,000 MPa, and the Poisson's ratio of ν = 0.3 are considered for used steel in the device. The two fixed supports in both ends of the device are modeled as fully restrained. To augment the accuracy of the modeling, a small mesh of 10 mm is used, and the radial force applied to the center of the quarter-ring is in the form of displacement control.

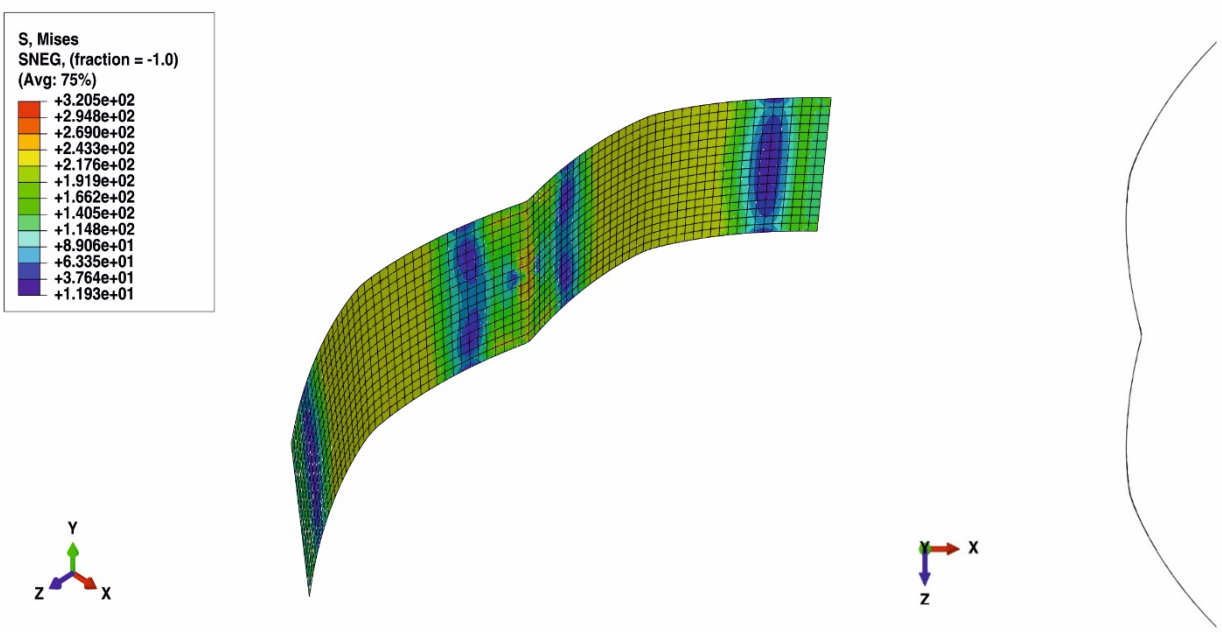

Fig. 14. Deformations in the FE model of the quarter-ring device (R=500 mm, b=150 mm, and t=10) subjected to 45 degrees loading at its center.

The results presented in Fig. 14 indicate that the plastic curvature of the arcs AB′ and CB′ has a very small effect on the ΔL_{AB} and ΔL_{BC} values, but due to the remarkable amount of internal work carried out by axial forces in the device, these small changes in the lengths are not negligible (ΔL_{AB} and ΔL_{BC} are shorter than expected). Moreover, the variability of the axial force along the curved device makes it difficult to determine the internal work performed by this force. Therefore, to solve the problem, it is necessary to modify the work done by axial forces in virtual work relationship with a factor less than one (called X factor). To make this hypothesis and solution acceptable, it needs to be proved that the X factor shows little change in various designs, and can be considered as a constant factor in Eq. (35).

$$4M_P \times \frac{\sqrt{2R\alpha - \alpha^2}}{R} + 2.252F_2R\left(\frac{\pi}{4} - 2\arcsin\left[\sqrt{2-\sqrt{2}}\left(\frac{1}{2} - \frac{\Delta}{4R}\right)\right]\right)X = F_2\Delta \quad (35)$$

The value of the reduction factor X lies between 0.65 and 0.7. The proposed factor is thoroughly examined and justified through implementing parametric analyses in Section 6. Note that to use Eq. (35), it is necessary to calculate the value of the central displacement Δ.

5.2. Approximate solution

In the approximate solution, although there is no need to calculate the values of α and β, answers are exceptionally accurate. In this procedure, the relationship between the rotation θ and the displacement of node B, Δ, is expressed using the rigid body rotation law as follows:

$$\Delta_B = \Delta = AB \times \theta = R\sin 45^\circ \times \theta = \frac{\sqrt{2}}{2} R\theta \rightarrow \theta = \sqrt{2}\frac{\Delta}{R} \tag{36}$$

Utilizing Eq. (36), Eq. (35) can be manipulated as follows:

$$4M_P \times \sqrt{2}\frac{\Delta}{R} + 2.252F_2R(\frac{\pi}{4} - 2\arcsin[\sqrt{2-\sqrt{2}}(\frac{1}{2} - \frac{\Delta}{4R})])X = F_2\Delta \tag{37}$$

As previously recommended, the value of the reduction factor X is in the range of 0.65-0.7. It is noteworthy that Eq. (37) is not dependent upon the amount of the displacement Δ, and in the design of a quarter-ring device, with chosen values of R and b along with any desired value of Δ, the thickness corresponding to the maximum strength of the quarter-ring device can be simply obtained using this equation. Provided that the desired value of Δ is not selected extremely large ($\Delta \not> 7.2R$), and to be placed in the acceptable range of arcsine term. The applicability and accuracy of Eqs. (17) and (37) with the X factor, are established in Section 6 via drawing a comparison between analytical results and responses of developed formulas.

6. FE models of devices in ABAQUS

In the current section, considering the suggested limited ranges for geometric parameters of the steel device (R, b, and t), 36 finite element models are initially built in ABAQUS software [22] (according to the specimens provided in Fig. (15). Then by making use of the obtained force responses corresponding to the strength of the first flexural plastic hinge formation and maximum strength (related to the formation of three flexural plastic hinges) in each quarter-ring, the accuracy of the obtained thickness resulted from Eqs. (17) and (37) are controlled. Finite element modeling specifications of the quarter-rings as well as loading method were entirely explained in the previous section. The suggested limited ranges for geometric characteristics of the devices based on dimensional features of steel IPE beams (connected to the devices) and design suggestions recommended in previous sections, are presented below:

$$\begin{aligned} &5\,\text{mm} \le t \le 20\,\text{mm} \\ &200\,\text{mm} \le R \le 500\,\text{mm} \\ &100\,\text{mm} \le b \le 200\,\text{mm} \end{aligned} \tag{38}$$

As reported in Table 1, for the quarter-rings radius 200, 350, and 500 mm, for their width 100, 150, and 200 mm, and for their thickness 5, 10, 15, and 20 mm have been adopted. After conducting the 36 parametric analyses each of which meets the limitation sets, a comparison between numerical results and responses from Eqs. (17) and (37) are drawn in Table 1.

Table 1
Comparison between numerical results and developed formulas

Model number	Radius of the device, R (mm)	Width of the device, b (mm)	Thickness of the device, t (mm)	F_1 (N)	F_2 (N)	Estimated thickness by Eq. (17) (mm)	Estimated thickness by Eq. (37) and X=0.65 (mm)
1	200	100	5	10062.7	13597.4	5	5.62
2	200	100	10	41719.5	51835.1	10.33	10.96
3	200	100	15	94000	109797	15.85	15.95
4	200	100	20	163000	181230	21.46	20.54
5	200	150	5	12400	24474.9	4.5	6.17
6	200	150	10	50000	85743.6	9.2	11.56
7	200	150	15	112000	148883	14	15.25
8	200	150	20	195000	221340	18.91	18.57
9	200	200	5	12100	40971.9	3.9	6.93
10	200	200	10	52000	127161	8.1	12.25
11	200	200	15	126000	210598	12.8	15.75
12	200	200	20	205000	299433	16.6	18.8

13	350	100	5	6700	7604.48	5.38	5.58
14	350	100	10	28000	32825.6	11	11.57
15	350	100	15	61425	72013.2	16.5	17.1
16	350	100	20	105000	122681	21.85	22.33
17	350	150	5	8500	11515.8	4.95	5.58
18	350	150	10	38000	47286.4	10.52	11.31
19	350	150	15	87000	104974	16	16.94
20	350	150	20	158000	180743	21.8	22
21	350	200	5	10000	16419.5	4.65	5.77
22	350	200	10	44000	61524.2	9.8	11.18
23	350	200	15	101000	127278	15	16
24	350	200	20	180000	211091	20.15	20.72
25	500	100	5	4254	4854.9	5.12	5.3
26	500	100	10	18600	22012.4	10.74	11.3
27	500	100	15	42000	50913.8	16.21	17.21
28	500	100	20	70000	88627.4	21	22.7

29	500	150	5	5850	7429.6	4.91	5.36
30	500	150	10	26000	33232.7	10.37	11.34
31	500	150	15	61000	76972.9	15.95	17.3
32	500	150	20	110000	134267	21.54	22.8
33	500	200	5	7050	10207.8	4.66	5.43
34	500	200	10	34500	43881	10.34	11.28
35	500	200	15	75000	100133	15.31	17
36	500	200	20	136000	176366	20.72	22.86

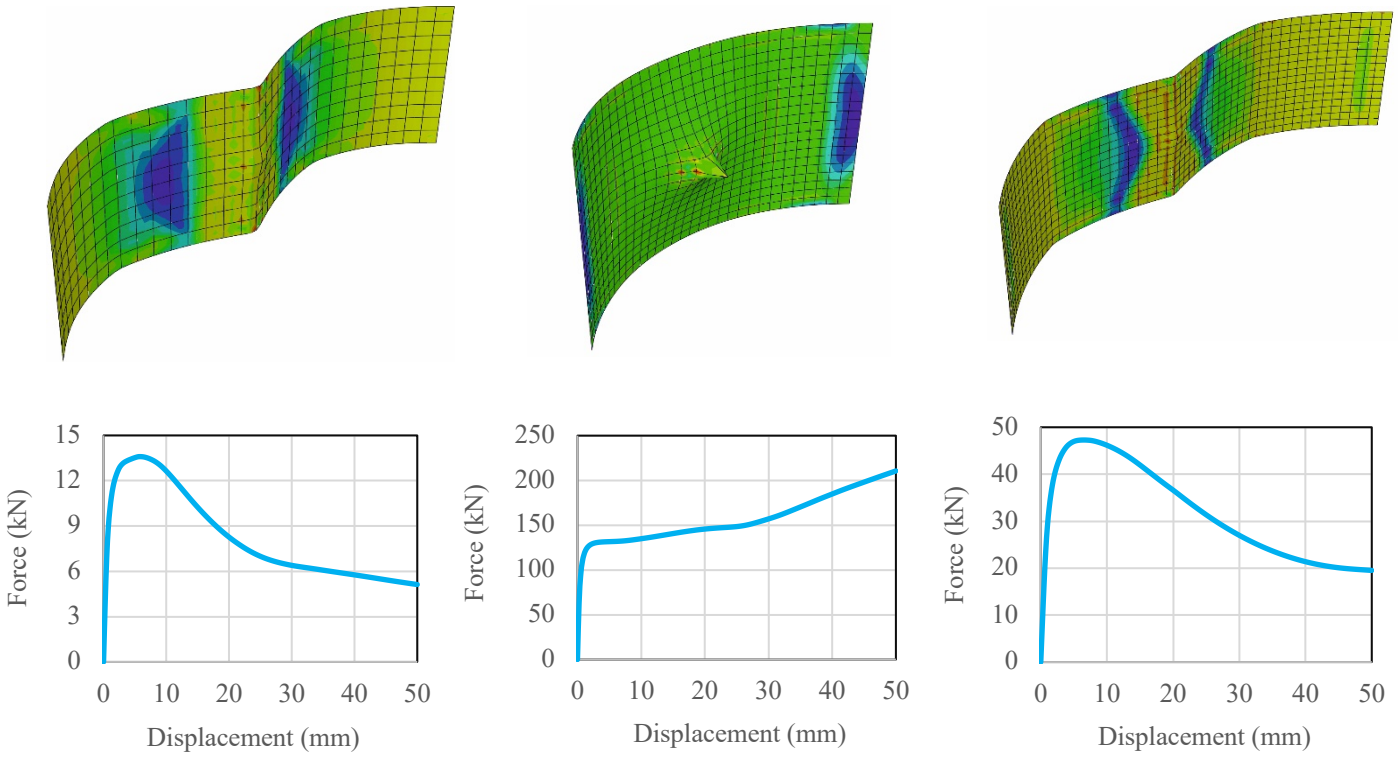

(a) (b) (c)

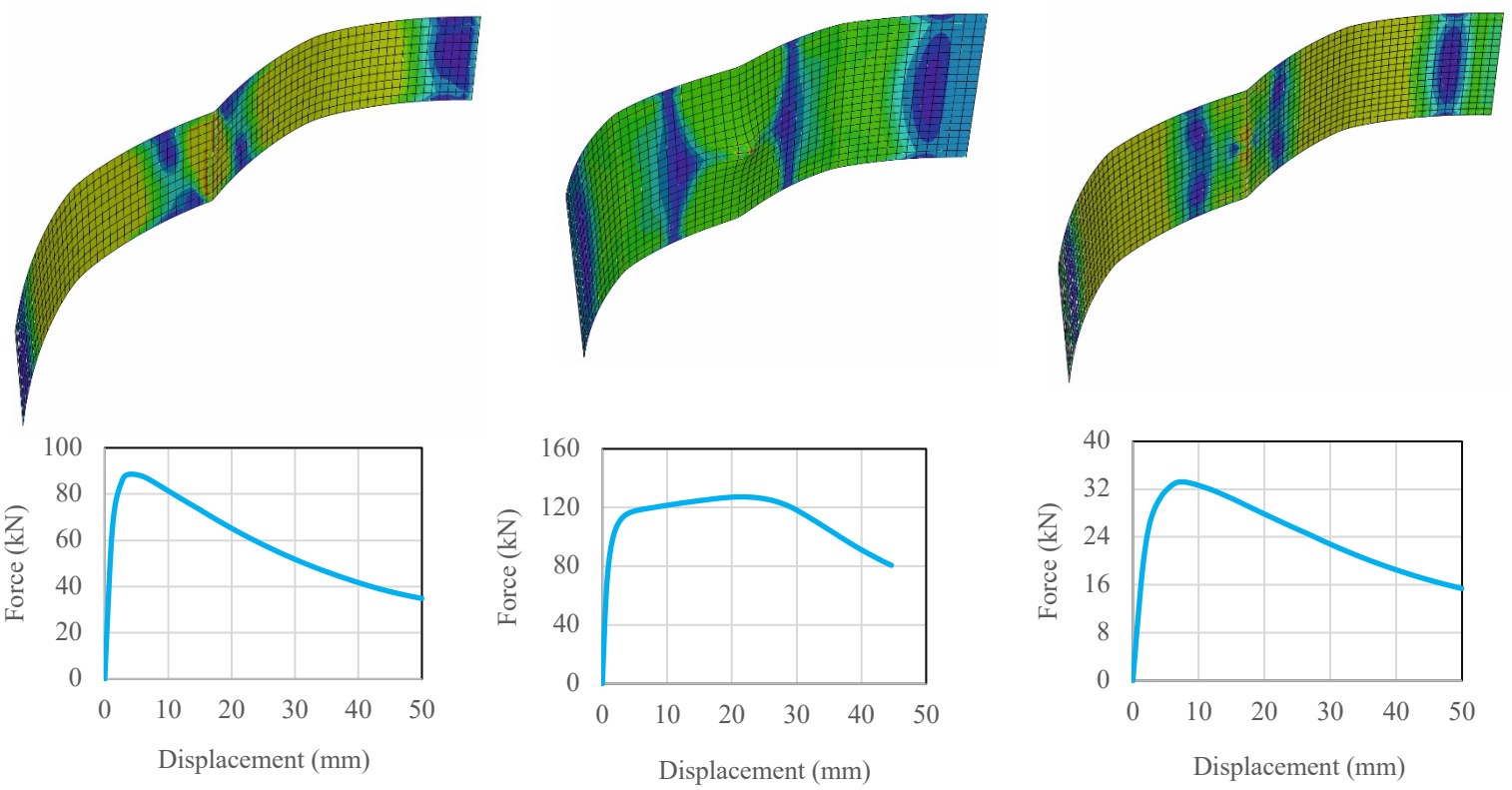

(d) (e) (f)

Fig. 15. FE models of devices subjected to loading at their center with their force-displacement diagram: (a) R=200 mm, b=100 mm, t=5 mm, (b) R=200 mm, b=200 mm, t=15 mm, (c) R=350 mm, b=150 mm, t=10 mm, (d) R=500 mm, b=100 mm, t=20 mm, (e) R=350 mm, b=200 mm, t=15 mm, and (f) R=500 mm, b=150 mm, t=10 mm.

As observed in Table 1, both Eqs. (17) and (37) with the reduction coefficient of X=0.65, are capable of accurately predicting the thickness of the 36 modeled devices with a low percentage of error and close approximation. As an example to clarify the problem, the device thickness for model 1 computed using Eq. (35) having $\Delta = 5.75$ mm and $\alpha = 0.1671$ (calculated using Eq. (26)), is equal to 5.6 mm. In addition, the obtained results demonstrate that by keeping the ultimate strength to be constant (i.e. the radial force F_2 value) in two distinct cases of devices reported in Table 1 (for example case 2 with 27, and case 16 with 23), a

reduction in radius R and an increase in device width b, bring about a decrease in the required thickness. For further assurance, the calculated thickness can be rounded to the greater value.

7. FE model of a portal moment frame endowed with a cable-cylinder bracing system and devices

In this section, in order to investigate the effects of devices' behavior on the performance of the cable-cylinder bracing system, the portal moment frame experimented by Hou and Tagawa [2] is meticulously modeled and verified using ABAQUS finite element software [22]. Subsequently, the quarter-ring devices designed based on frame characteristics are added to the system, and the performance of new lateral load resisting system is compared with that of conventional cable-cylinder bracing system. As illustrated in Fig. 16, the frame examined by Hou and Tagawa [2] utilized similar beam and column sections of H-150x150x7x10, which have T-stub connections as H-300x150x6.5x9 made of SS400 steel.

The existing bracing members in this system are stainless steel (SUS316) strand (7×19) cables passing through a steel pipe (high-stiffness pipe) with 214 mm length, 40 mm inner diameter, and 15 mm thickness. The geometric dimensions of this steel pipe have been calculated based on the drift in which the cables start acting which is considered equal to 30 mm in this experiment. The tensile force corresponding to cables yielding has been reported approximately equal to 58 kN in this sub-assembly as well. Given the difference of lower than 10 degrees between the cable direction and radial direction of the devices ($\cos 10^{\circ} \simeq 1$), using Eq. (37) with X=0.65 and 58 kN F_2 force leads to the minimum required thickness of the devices to be estimated as15mm. The radius and width of each device are considered as 300 mm and 200 mm, respectively.

LYP steel having yielding stress of about 100 MPa and E=200000 MPa (used in [15]), is used as devices' material.

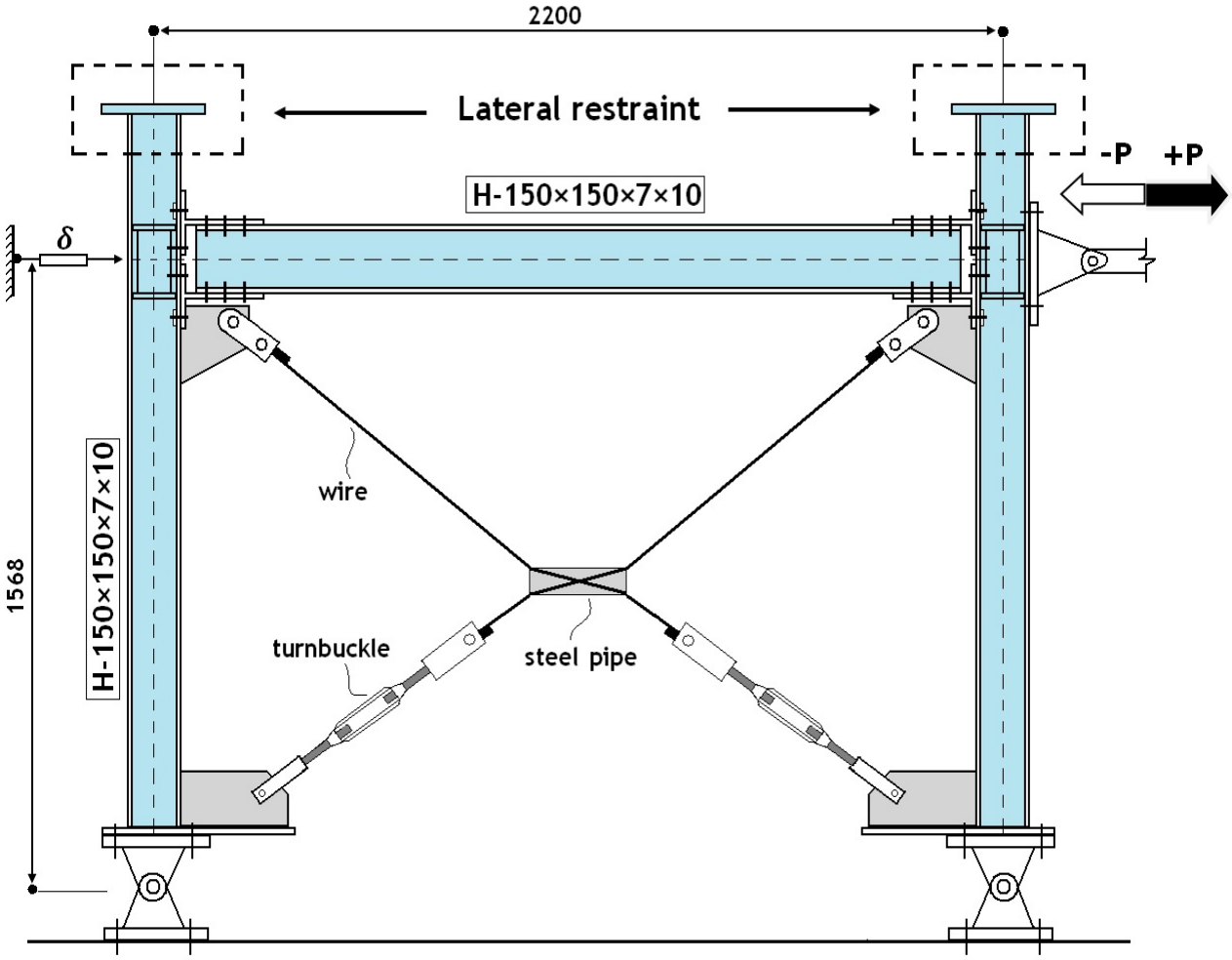

Fig. **16.** Portal moment frame subassembly endowed with a cable-cylinder bracing system after Hou and Tagawa [2].

Finite element samples have been modeled considering continuity and doubler plates, column stiffeners, gusset plates, and base plates which are completely compatible with the experimental ones (Fig. 17). The thickness of baseplates is determined to mobilize enough stiffness providing full plastification of the connected quarter-ring devices during cyclic loading. Out-of-plane displacement of the desired frame has been restricted at the column tops. Both supports in the models have been considered as pinned. The beam and columns need to remain

elastic during the experiment, therefore, their material properties have been considered as perfectly elastic in modeling. To model wire ropes, the wire element possessing the beam section has been employed, and the central steel pipe has been considered as a rigid shell cylinder. In the modeling of other members, the solid element has been utilized. In order to enhance the accuracy of the modeling responses, C3D2OR element which is an excellent general-purpose element, and rarely exhibits hour-glassing despite the reduced integration, has been utilized in both T-stubs and devices.

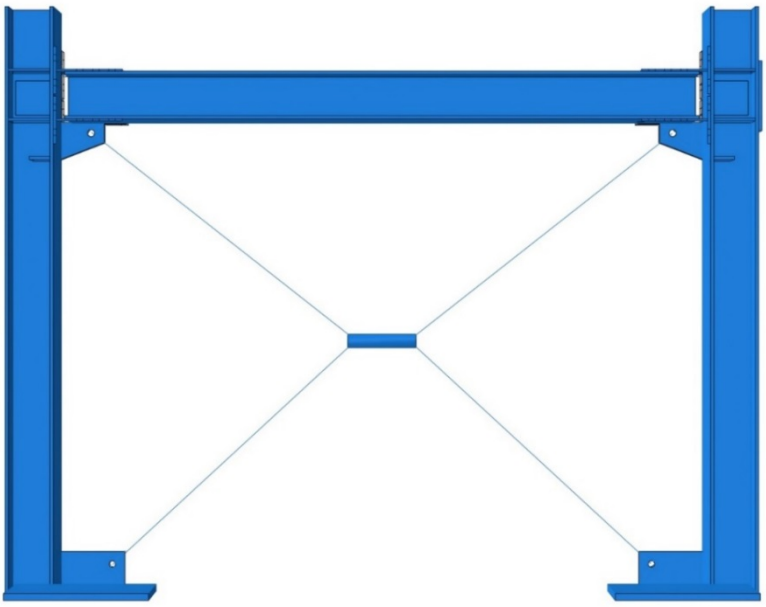

(a)

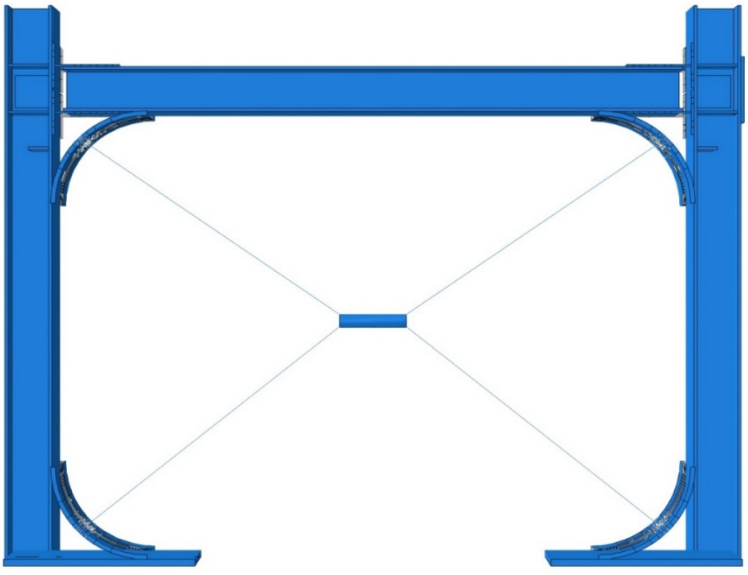

(b)

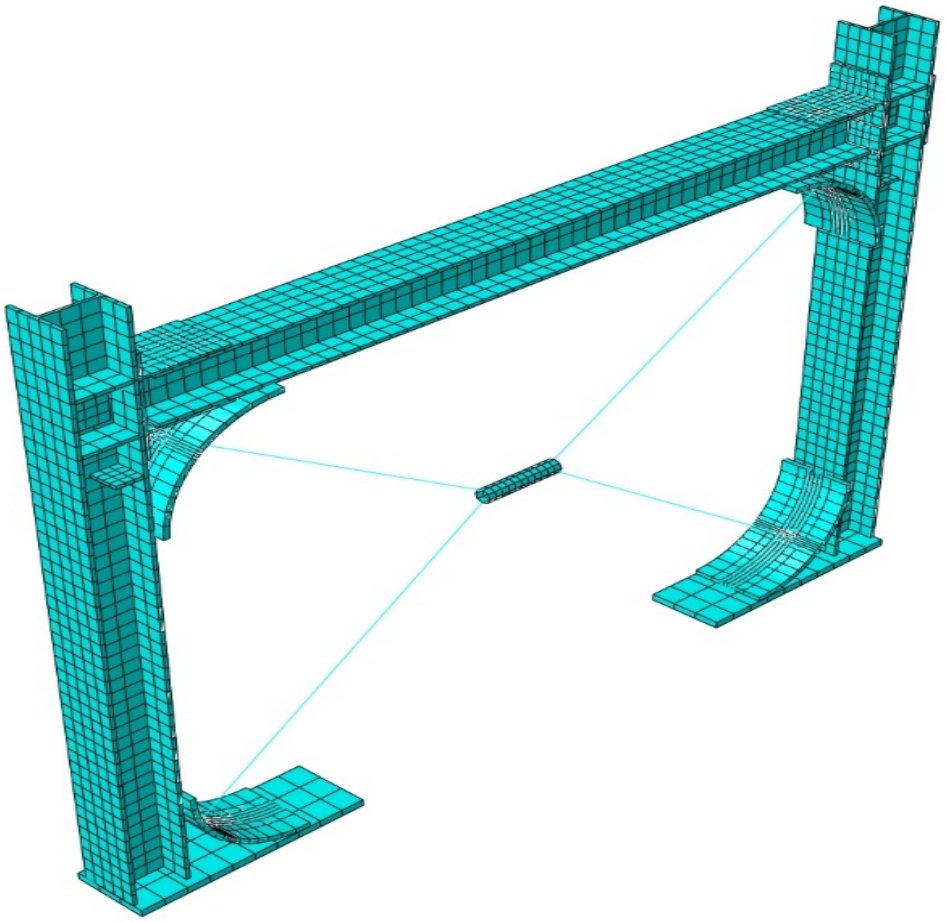

(c)

Fig. 17. FE models: (a) portal moment frame with a cable-cylinder bracing system tested by Hou and Tagawa [2]; (b) the proposed system equipped with curved yielding devices, and (c) an example of a FE model.

To avoid the problem of convergence in results, frictionless surface interaction has been adopted at the T-stub connections. As shown in Fig.18, cyclic loading applied to finite element models is a displacement-controlled loading protocol completely consistent with the one implemented in the experiment.

Fig. **18.** Displacement-controlled loading protocol applied to the experimental specimen as well as finite element model.

In the experiment, the cables were ruptured in the lateral drift of 80 mm, and then the experiment was stopped. The finite element modeling verification is presented in Fig. 19. As it is observed, the finite element model shows a high level of precision and agreement.

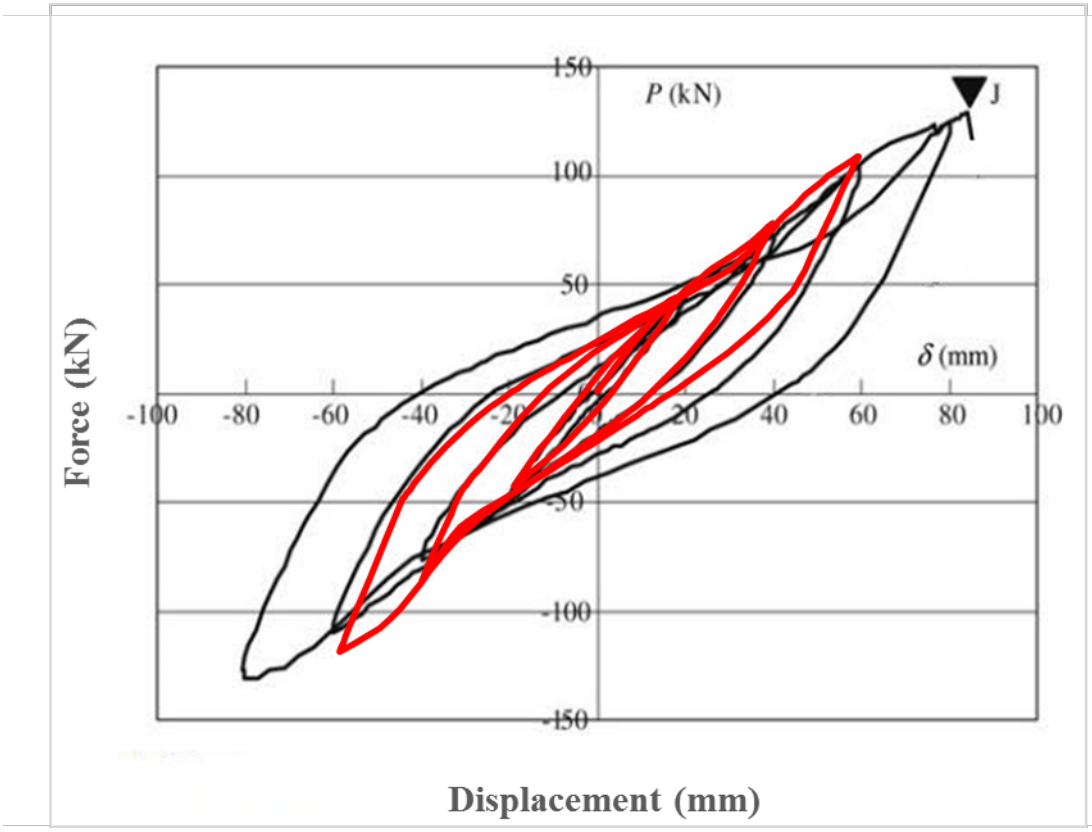

Fig. 19. Hysteresis behavior verification of the modeled cable-cylinder bracing system.

Improvement in the cyclic behavior of the cable-cylinder bracing system after designed yielding devices are added, is depicted in Fig. 20.

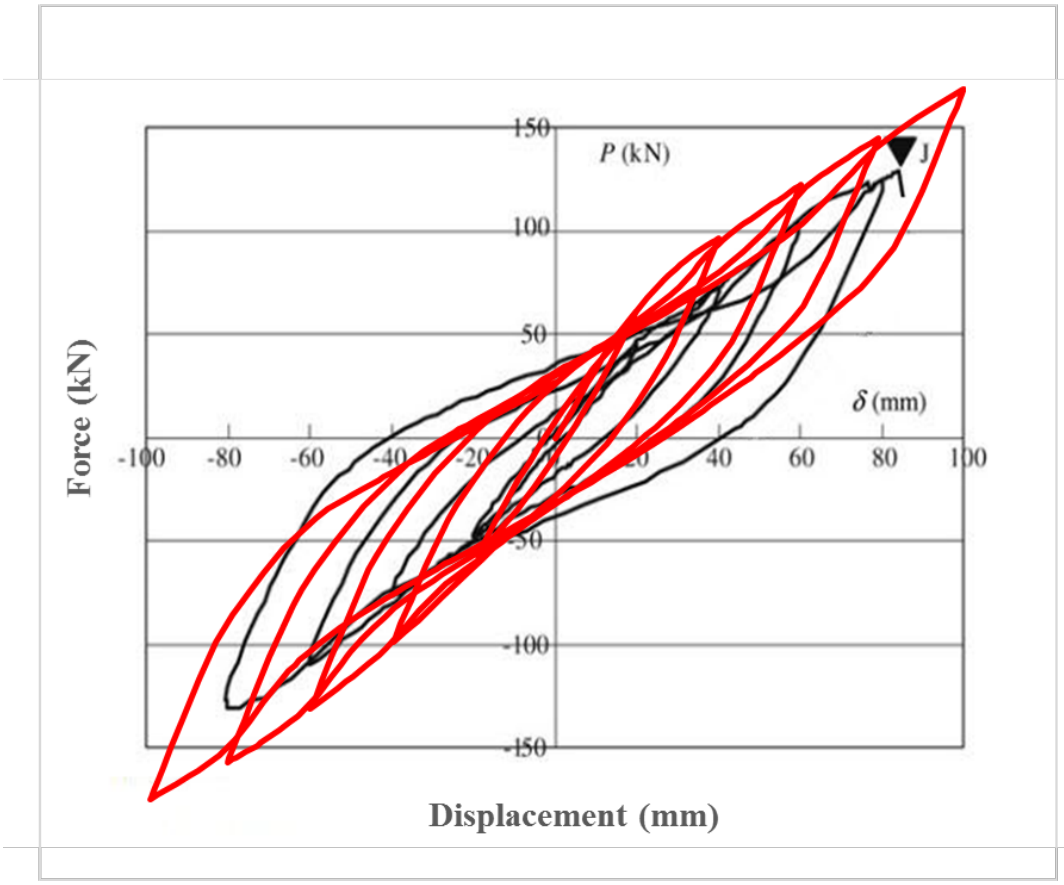

Fig. 20. Comparison of hysteresis behavior between the conventional cable-cylinder bracing system examined by Hou and Tagawa [2] and the proposed system in this study.

Regarding the obtained results from the modeled frame with and without curved yielding devices, it is concluded that the designed devices are capable of modifying efficiently and dramatically enhancing the system behavior. Fig. 21 depicts the backbone curves of both systems. Table 2 shows that these devices have endowed the cable-cylinder bracing system with 37% increase in ultimate strength, 36% increase in initial stiffness, 31% increase in ductility (the ratio of ultimate displacement to the initial yield displacement), and conspicuous 130% increase in energy dissipation of the system. The simultaneous increase in stiffness and strength along with energy dissipation (in an exceptional amount) is

reckoned as one of the special merits of the new system since the stiffness and energy dissipation are usually inversely proportionate. Installing quarter-ring devices made of LYP steel into the previous system has also significantly alleviated the influence of pinching behavior observed in the experiment (shown in Fig. 20). Furthermore, increasing the tolerable drift of the system from 80 mm to 100 mm, preventing the rupture of cables connected to the beam-to-column connections due to early yielding of the devices, and finally upgrading overall performance level of the system were discovered from the responses.

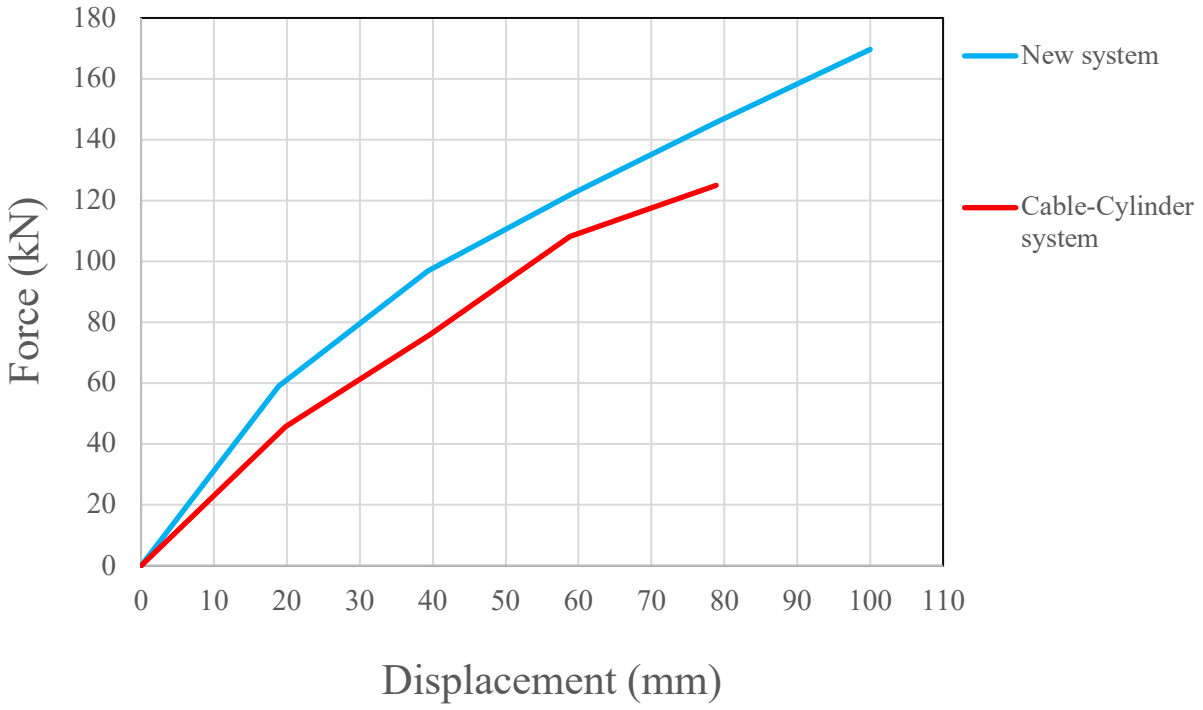

Fig. 21. Comparison of backbone curves in the ring-cable-cylinder system and the cable-cylinder bracing system experimented by Hou and Tagawa [2].

Table 2
Comparison between proposed system with conventional cable-cylinder bracing system

Systems ratio	Ultimate strength (kN), ratio	Initial stiffness (kN/m), ratio	Dissipated energy (kJ), ratio	Ductility ratio
New system/Conventional system	$\frac{169.69}{124.16} = 1.37$	$\frac{3122.28}{2302.07} = 1.36$	$\frac{57.18}{24.84} = 2.3$	$\frac{5.29}{4.03} = 1.31$

8. Conclusions

In the current study, a new cable-cylinder bracing system equipped with replaceable curved yielding devices was initially introduced. It can remarkably improve both stiffness and strength characteristics of the bracing system and add both ductility and energy dissipation to the structure. Along this vein, a set of equations was derived based on least and virtual work methods with design recommendations so as to design the quarter-ring device and compute its thickness in two distinct cases: i) the initial formation of a flexural plastic hinge; ii) the subsequent formation of three plastic hinges at ultimate strength. The accuracy of the proposed equations was assessed by performing 36 FE analyses. In the final part of the paper, the performance of a portal steel moment frame endowed with the proposed cable-cylinder bracing system was verified under cyclic loading. The most significant results of this study are outlined below:

1. The novel cable-cylinder bracing system equipped with replaceable curved yielding devices can be easily implemented at low cost in frames vulnerable to lateral forces. Furthermore, the system is very flexible, being replaceable or modifiable after each earthquake.
2. The proposed system can localize damage in the bracing system, prevent damage in beam-to-column connections and postpone failure of the cable-

cylinder bracing system due to early yielding of quarter-ring devices made of low-yield-point steel.

3. Both the arch action and the use of low-yield-point steel in devices, lead to a decrease of local buckling, the reduction of compactness ratio and an increase in the long-term cyclic stability of the system.

4. Two novel equations allow for a reliable estimation of the required thickness of the quarter-ring devices in two significant cases of one flexural plastic hinge and three plastic hinges at ultimate strength, respectively. They do not depend on the middle radial displacement of the ring. It is recommended that the device width must not exceed 1.25 times the smallest value of beam and column flange width. Moreover, the device radius must be considered in the range of 200 to 500 mm.

5. The parametric analysis indicates that for a constant ultimate strength of the devices which corresponds to the yielded cable force, both a reduction of device radius and an increase in device width entail a thickness decrease.

6. The application of the new cable-cylinder bracing system equipped with replaceable curved yielding devices to the moment frame cyclically tested by Hou and Tagawa [2] entails a 36% gain in initial stiffness, a 37% increase in ultimate strength, , a 31% gain in ductility, and a noticeable 130% increase in energy dissipation together with a significant reduction of adverse pinching. Finally, a deep assessment of the proposed bracing system with a focus on realistic earthquake demands on several braced frame geometries deserves further studies.

Acknowledgement

This work received support from the Italian Ministry of Education, University and Research (MIUR) in the frame of the ‘Departments of Excellence’ (grant L 232/2016) for the first author.

References

[1] H. Tagawa, X. Hou, Seismic retrofit of ductile moment resisting frames using wire-rope bracing, Proceedings of the Eighth Pacific Conference on Earthquake Engineering, 2007.
[2] X. Hou, H. Tagawa, Displacement-restraint bracing for seismic retrofit of steel moment frames, Journal of Constructional Steel Research 65(5) (2009) 1096-1104.
[3] S. Aghajani, Assessment of behaviour of steel frames with cable bracing, Master thesis, Under supervision of Dr. Nader Fanaie, K. N. Toosi University of Technology, 2011.
[4] N. Fanaie, S. Aghajani, E.A. Dizaj, Theoretical assessment of the behavior of cable bracing system with central steel cylinder, Advances in structural engineering 19(3) (2016) 463-472.
[5] N. Fanaie, S. Aghajani, E. Afsar Dizaj, Strengthening of moment-resisting frame using cable–cylinder bracing, Advances in structural engineering 19(11) (2016) 1736-1754.
[6] N. Fanaie, S. Aghajani, Wire-rope bracing system with central cylinder, element based application finite element based application, Proc. 15th World Conference on Earthquake Engineering, Lisbon, 2012.
[7] N. Fanaie, N. Zafari, Sensitivity Analysis on Response Modification Factor of New Cable-Cylinder Bracing Systems, Journal of Earthquake Engineering 23(4) (2019) 648-668.
[8] S. Beheshti-Aval, H. Mahbanouei, F. Zareian, A hybrid friction-yielding damper to equip concentrically braced steel frames, International Journal of Steel Structures 13(4) (2013) 577-587.
[9] K. Deng, P. Pan, C. Wang, Development of crawler steel damper for bridges, Journal of Constructional Steel Research 85 (2013) 140-150.
[10] S. Maleki, S. Mahjoubi, Dual-pipe damper, Journal of Constructional Steel Research 85 (2013) 81-91.
[11] J. Utomo, M. Moestopo, A. Surahman, D. Kusumastuti, Estimating the ultimate energy dissipation capacity of steel pipe dampers, Procedia Engineering 125 (2015) 1101-1107.
[12] Z. Andalib, M.A. Kafi, A. Kheyroddin, M. Bazzaz, Experimental investigation of the ductility and performance of steel rings constructed from plates, Journal of Constructional steel research 103 (2014) 77-88.

[13] F. Taiyari, F.M. Mazzolani, S. Bagheri, A proposal for energy dissipative braces with U-shaped steel strips, Journal of Constructional Steel Research 154 (2019) 110-122.
[14] Y. Chen, C. Chen, H. Jiang, T. Liu, Z. Wan, Study of an innovative graded yield metal damper, Journal of Constructional Steel Research 160 (2019) 240-254.
[15] M. Shariati, S.S. Faegh, P. Mehrabi, S. Bahavarnia, Y. Zandi, D.R. Masoom, A. Toghroli, N.-T. Trung, M.N. Salih, Numerical study on the structural performance of corrugated low yield point steel plate shear walls with circular openings, Steel and Composite Structures 33(4) (2019) 569-581.
[16] A. Al Kajbaf, N. Fanaie, K.F. Najarkolaie, Numerical simulation of failure in steel posttensioned connections under cyclic loading, Engineering Failure Analysis 91 (2018) 35-57.
[17] S.-J. Chen, C. Jhang, Experimental study of low-yield-point steel plate shear wall under in-plane load, Journal of Constructional Steel Research 67(6) (2011) 977-985.
[18] C. Zhang, T. Aoki, Q. Zhang, M. Wu, Experimental investigation on the low-yield-strength steel shear panel damper under different loading, Journal of Constructional Steel Research 84 (2013) 105-113.
[19] N. Fanaie, S.S. Faegh, F. Partovi, An improved and innovative formulation for calculating amplified elastic story drift induced by RBS connections in steel moment frames, Journal of Constructional Steel Research 160 (2019) 510-527.
[20] N. Fanaie, M. Tahriri, Stability and stiffness analysis of a steel frame with an oblique beam using method of least work, Journal of Constructional Steel Research 137 (2017) 342-357.
[21] W. Chen, D. Han, Plasticity for structural engineers. 1988, Springer, New York.
[22] A. Version, 6.14-1. Dassault Systémes Simulia Corp, Providence, RI (2014).